HHS Public Access

Author manuscript

J Immunol. Author manuscript; available in PMC 2018 July 01.

Published in final edited form as:

J Immunol. 2018 January 01; 200(1): 147–162. doi:10.4049/jimmunol.1701087.

A Novel *Pkhd1* mutation interacts with the Nonobese diabetic (NOD) genetic background to cause autoimmune cholangitis

Wenting Huang[*,1], **Daniel B. Rainbow**[†,1], **Yuehong Wu**[*], **David Adams**[*], **Pranavkumar Shivakumar**[‡], **Leah Kottyan**[§], **Rebekah Karns**[‖], **Bruce Aronow**[‖], **Jorge Bezerra**[‡], **M. Eric Gershwin**[#], **Laurence B. Peterson**[**], **Linda S. Wicker**[†], and **William M Ridgway**[*]

[*]Division of Immunology, Allergy and Rheumatology, University of Cincinnati College of Medicine, Cincinnati Ohio, 45267

[†]JDRF /Wellcome Trust Diabetes and Inflammation Laboratory, Wellcome Trust Center for Human Genetics, Nuffield Department of Medicine, National Institute for Health Research Oxford Biomedical Research Centre, University of Oxford, Roosevelt Drive, Oxford, OX3 7BN, UK

[‡]Division of Pediatric Gastroenterology, Hepatology and Nutrition, Cincinnati Children's Hospital Medical Center, Cincinnati OH, 45229

[§]Department of Pediatrics, Cincinnati Children's Hospital Medical Center, Cincinnati OH, 45229

[‖]Division of Biomedical Informatics, Cincinnati Children's Hospital Medical Center, Cincinnati OH, 45229

[#]Division of Rheumatology, Allergy and Clinical Immunology, University of California at Davis, Davis CA 95616

[**]Department of Pharmacology, Merck Research Laboratories, Rahway, NJ 07065

Abstract

We previously published that NOD.c3c4 mice develop spontaneous autoimmune biliary disease (ABD) with anti-mitochondrial antibodies, histopathological lesions, and autoimmune T lymphocytes similar to human primary biliary cholangitis (PBC). Here we demonstrate that ABD in NOD.c3c4 and related NOD ABD strains is caused by a chromosome 1 region that includes a novel mutation in Polycystic kidney and hepatic disease 1 (*Pkhd1*). We show that an LTR element inserted into intron 35 exposes an alternative polyadenylation site, resulting in a truncated *Pkhd1* transcript. A novel NOD congenic mouse expressing aberrant *Pkhd1*, but lacking the c3 and c4 chromosomal regions ("NOD.*Abd3*"), reproduces the immunopathological features of NOD ABD. RNA-seq of NOD.*Abd3* common bile duct early in disease demonstrates upregulation of genes involved in cholangiocyte injury/morphology and downregulation of immunoregulatory genes. Consistent with this, bone marrow chimera studies show that aberrant *Pkhd1* must be expressed in both the target tissue (cholangiocytes) and the immune system (bone marrow). Mutations of *Pkhd1* produce biliary abnormalities in mice, but have not been previously associated with autoimmunity. Here we eliminate clinical biliary disease by backcrossing this *Pkhd1* mutation onto the B6

Corresponding author: William M Ridgway; Telephone: 513-558-4701; Fax: 513-558-3799; ridgwawm@ucmail.uc.edu.

[1]These two authors contributed equally to the manuscript

genetic background: thus the NOD genetic background (which promotes autoimmunity) is essential for disease. We propose that loss of functional *Pkhd1* on the NOD background produces early bile duct abnormalities, initiating a break in tolerance that leads to autoimmune cholangitis in NOD.*Abd3* congenic mice. This model is important for understanding loss of tolerance to cholangiocytes and is relevant to the pathogenesis of several human cholangiopathies.

Introduction

Autoimmune biliary disease (ABD) in humans includes primary biliary cholangitis (PBC) and primary sclerosing cholangitis in adults (1-3) and biliary atresia in children (4, 5). The biliary epithelial cell (cholangiocyte) is the main autoimmune target in these diseases (6, 7). Several animal models of ABD have been established. NOD.c3c4 (8, 9), NOD.ABD (10), and dnTGFβRII mice (11) develop spontaneous ABD similar to PBC. Infection of neonatal BALB/c mice produces an autoimmune reaction very similar to biliary atresia (7, 12). The NOD.c3c4 strain arose in a project to refine Insulin-Dependent Diabetes (*Idd*) loci by introgressing B6 and B10 *Idd* regions onto the NOD genetic background (8). We showed that NOD.c3c4 mice are completely protected from diabetes, but develop ABD characterized by hepatosplenomegaly, wasting, abdominal swelling, liver function abnormalities, and eventually death from obstructive liver disease. Histologically their livers show substantial lymphocytic infiltration, nonsuppurative destructive cholangitis, and macrophage aggregation in the bile ducts; all features similar to human PBC. In addition, NOD.c3c4 mice spontaneously develop anti-Pyruvate Dehydrogenase E2 autoantibodies (anti-mitochondrial antibodies), which are highly specific for human PBC. In contrast to human PBC, NOD.c3c4 mice also develop common bile duct dilation and inflammation, which more closely resembles primary sclerosing cholangitis or biliary atresia. Finally, they develop extensive proliferation of intrahepatic bile ductules, far exceeding the ductule proliferation seen in stage II human PBC and more resembling polycystic liver disease (8, 9, 13). Transfer of splenocytes from NOD.ABD donors with severe disease, however, resulted in overwhelming inflammation, nonsuppurative destructive cholangitis, high titer anti-Pyruvate Dehydrogenase E2 antibodies, and severe illness in NOD.c3c4-*scid* recipients—in the absence of any additional significant ductular proliferation (10). We concluded that the NOD.c3c4 mouse strain was a useful model for understanding the mechanisms of autoimmune biliary disease.

We have previously identified several immune mechanisms of NOD autoimmune biliary disease. First, NOD.c3c4-*scid* mice do not develop clinical disease and have much diminished hepatic histological abnormalities, indicating that the adaptive immune system is critical to disease pathogenesis (10). Second, CD8 T cells from NOD.ABD donors, but not NOD donors, transferred disease into NOD.c3c4-*scid* recipients (10). Finally, NOD-*scid* recipients did not develop ABD upon adoptive transfer, even when receiving 20 million splenocytes from NOD.ABD donors that rapidly caused overwhelming ABD in NOD.c3c4-*scid* recipients (10). These results showed that the genetic background of the target tissue was critical to disease pathogenesis, however the meaning of the requirement of B6/B10 genetic components in the adaptive immune system was unclear. An alternate explanation of our results was that NOD splenocytes did not cause disease because autoreactive,

cholangiocyte-directed T cells were not expanded, due to T cell repertoire development in the absence of the cholangiocyte autoantigen(s). This issue is addressed in the current paper by constructing bone marrow chimeric mice.

We used a congenic mapping approach to define the genetic origin of ABD in the NOD.c3c4 model (10). Although regions on chromosomes 3 and 4 were initially linked to disease, a genome-wide 5K SNP chip analysis showed a small non-NOD region on chromosome 1 in all strains that developed disease. In order to assess the role of this region we constructed a new chromosome 1 congenic strain, herein designated NOD.*Abd3*. The NOD.*Abd3* strain develops highly penetrant ABD, similar to the previously described strains, in the absence of the original chromosome 3 and 4 congenic regions present in either the NOD.c3c4 or NOD.ABD models. We undertook the studies in the present paper to understand how the chromosome 1 genetic region mediates biliary disease, and to further characterize the role of genetic background and the chromosome 1 region in the target tissue (biliary epithelium) and hematopoietic system. From these investigations we discovered the congenic region on chromosome 1 is itself unlikely to cause ABD, but rather the highly likely cause is a mutation altering the expression of a gene closely linked (2.5 Mb) to the congenic region, Polycystic kidney and hepatic disease 1 (*Pkhd1*).

Materials and Methods

Animals and genotyping

NOD, NOD.ABD (14), NOD.CD45.2 (15), B10.H2^{g7}, B6.PL-Thy1a/CyJ (hereafter termed “B6.PL”), and B6 mice and mice derived therefrom during this study were bred and housed under specific pathogen-free conditions, and all procedures were conducted according to approved protocols of the University of Cincinnati College of Medicine or the Merck Research Laboratories Animal Care and Use Committees. We discovered during quality control screening of congenic strains in our colony, using a 5K mouse single nucleotide polymorphism (SNP) chip (ParAllele Biosciences, South San Francisco, CA), that the NOD.c3c4 (9) and NOD.ABD strains included a non-NOD-derived congenic region (derived from either the B6.PL or B10 mouse strains) on chromosome 1 (Supplemental Table 1). This region was isolated by selective backcrossing to NOD as line 7825 (N11) (Fig 1). Line 7825 was used to generate additional chromosome 1 recombinants to isolate smaller congenic segments resulting in lines NOD.*Abd3* (line 8706, N13), 8727 (N11), 8728 (N11), and 8730 (N11) (Fig 2A). Novel primers developed to screen for recombination events and to define recombination points in detail are listed in Supplemental Table 2. To assess whether the NOD MHC contributed to ABD, line 7825 mice were bred to NOD.B10-*H2*^{b} (NOD.*H2*^{b}) mice (16) and then backcrossed to line 7825. Mice homozygous for the chromosome 1 congenic region and heterozygous for the *H2*^{b} MHC were intercrossed to fix both regions as homozygous for the non-NOD haplotype. Line 7825 mice were crossed to NOD, and the F1 mice were intercrossed to assess whether the *Abd3* region was recessive and sufficient to cause ABD on the NOD background in (7825 × NOD) F2 mice. A cohort of line 7825 mice was compared to a cohort of NOD mice for diabetes development as described (17). NOD.*Abd3* mice were crossed 1) once with B6 and then the F1 offspring were intercrossed to produce F2 mice, or 2) twice to B6 to generate Backcross 2 (BC2) mice, which were then

further intercrossed to generate the BC2 intercrossed (BC2i) generation. NOD.*Abd3* mice backcrossed to B6 were genotyped as follows using markers outside the B6 congenic region, which genotype as NOD for NOD.*Abd3* mice. The proximal marker is rs13475762 (Fig. 1A) with the forward primer rs13475762_F = TTCCCCCTTTTAATATTTTGCAT and reverse primer rs13475762_R = CAGGGAGGCAGTGATTTAGC. The distal marker is rs32040516 with forward primer rs32040516_F = TGAGCCATCTGACAGACCAG and reverse primer rs32040516_R = TGGATGGCCATGACAAAAA. PCR product was digested with restriction enzyme ACC1 (for proximal marker) or MNL1 (for distal marker) (New England Biolabs) at 37°C for 2 hours and the PCR products were run on a 4% agarose gel with 1× TBE buffer. The size of the digested PCR product of proximal markers is 87 bp for NOD and the size of the digested PCR product of distal markers is 182 bp. Comparison of NOD and B6 genomic sequence in the congenic portion of the *Abd3* region was performed as described (18).

Histopathology and disease scoring

Livers and/or common bile ducts were scored for visible/clinical liver and common bile duct pathology as previously described (8-10) (see below for methods), isolated from mice, immediately fixed in 10% formalin, and subsequently embedded in paraffin. Samples were stained with hematoxylin and eosin, and histology was scored blindly using microscopy for duct epithelial hyperplasia and lymphocytic infiltration.

Common bile duct (CBD) and liver gross pathological scoring—CBD dilation and the quantitation of liver abnormalities were examined and scored separately. The clinical liver score performed at UC was assigned based on tissue induration (hardness) and the presence of cysts on the surface of liver as follows: 0: soft and no cysts; 1: mild induration, no cysts; 2 indurated with cysts on one lobe surface; 3 indurated with cysts on two to three lobes; 4 indurated and cysts on all four lobes. The clinical CBD score was identical to the diameter (in mm) of the maximum CBD width; in the case of CBD 1< mm (“normal” CBD) the score was assigned as zero. The clinical biliary/liver score performed at Merck (on 7825 × NOD F2 mice) was assigned as follows: CBD, 0: normal; 1: size just above normal; 2: CBD clearly enlarged, but less than 2 mm; 3: CBD ~ 2 mm; 4:CBD ~2-4 mm; 5: CBD > 4 mm. Liver: 0: normal; 1: very few cysts in the liver; 2: cysts in liver are easily seen; 3:many cysts easily seen; 4: many cysts in most or all lobes; 5: liver completely full of cysts.

Histological liver score: duct epithelial hyperplasia

0 = 0~3 ductules per portal triad across the section

1 = a.) at least 2 times the normal diameter of ductule lumen in 10% ~ 25% of the entire section. b.) no fewer than 3 small ductules around one triad in 25% ~ 50% of the entire section.

2 = enlarging ductules across 25% ~ 50% of the entire section. The average diameter of a ductule lumen section is about 2~4 times of the normal ductule diameter

3 = larger ductules across >50% of the entire section. The average diameter of ductule lumen section is about 4~5.5 times of the normal ductule diameter

4 = dilated, diffuse, torturous ducts (“cysts”) in much of the section; this is the endstage disease. The average diameter of ductule lumen section is more than 5.5 times the normal ductule diameter

Histological score: leukocytic infiltration of portal areas

0 = none or a few cells in <25% of entire section;

1= small numbers of cells in multiple areas (25% ~ 50%), including some clusters of immune cells;

2 = small numbers of cells (a few cells thick infiltrate) diffusely (>50% of entire section); or patchy moderate infiltrates (25%~50% of entire section);

3 = moderate numbers of cells diffusely (>50% of entire section) or patchy large infiltrates (larger cluster than what is described in “2”, 25%~50% of entire section);

4 = diffuse or significant sections of large cellular infiltrates.

Bone marrow Chimeras

2~3-month-old NOD (CD45.1) or NOD.*Abd3* (CD45.1) mice were irradiated with 1200 Rads. 15~20 million bone marrow cells from 4-month-old NOD.CD45.2 or 2~3-month-old NOD.*Abd3* (CD45.1) donors were extracted without RBC lysis. Mature CD4, CD8 and CD90 cells were removed using magnetic beads (Miltenyl Biotech, California) and the bone marrow was injected i.v. into the irradiated recipient mice. Recipient mice were given water treated with antibiotic (neomycin trisulfate salt hydrate) for two weeks after transfer. The recipient mice were sacrificed 120 days post bone marrow transfer or when they developed abdominal swelling indicating severe hepatobiliary disease (approximately 2.5 months for NOD.*Abd3* recipients of NOD.*Abd3* bone marrow). Tissues were analyzed for anatomical and histological biliary/liver disease. CD45.1 or CD45.2 quantification was done for the recipients of different donor cells and the bone marrow reconstitution rate was from 87.6% to 98.9 %.

Quantitative real time PCR of mRNA

Extrahepatic common bile ducts were isolated from 2-week-old NOD.*Abd3* and NOD mice and stored in *RNAlater* solution (Qiagen). For RNA extraction from CBD, the tissue was first removed from *RNAlater* solution and disrupted in lysing/binding buffer provided in the mirVana™ miRNA Isolation Kit (Life Technologies) using a homogenizer (Qiagen) and then RNA was extracted from the tissues using mirVana™ miRNA Isolation Kit (Life Technologies) and converted to cDNA by random primers (High capacity cDNA Reverse Transcription kit, Applied Biosystems). Relative gene expression of *Pkhd1* was performed using selective mouse Taqman gene expression assays (Mm00467747_m1 for region spanning exon 35 and 36, Mm00467728_m1 for region spanning exon 15 and 16, Mm01233737_m1 for region spanning exon 60 and 61, Life Technologies) and endogenous control assay Rn18S (Mm03928990_g1, Life Technologies).

RNA-seq profiling of common bile ducts and data analysis

Total CBD RNA was extracted from 2-week-old NOD or NOD.*Abd3* mice using mirVana miRNA isolation kit (Life Technologies, CA). Two samples were sequenced for each strain; each of the two NOD.*Abd3* samples had RNA from three individual CBDs and the two NOD samples had RNA from three and five individual CBDs respectively. RNA concentration, purity (28S:18S rRNA ratio), and quality (RNA Integrity Number (RIN)) was assessed using the 2100 Bioanalyzer (Agilent, Santa Clara, CA) at the DNA Sequencing and Genotyping Core of Cincinnati Children's Hospital Medical Center. The RNA samples had a RNA integrity score (RIN) of at least 7.9 on the Agilent bioanalyzer (scale of 1 to 10 with 10 being completely intact).

The RNA sequencing library was generated with the Illumina TruSeq RNA preparation kit and subsequently sequenced on the Illumina Hi-Seq 2000, using single-end, 50-bp read specifications with a read depth of at least 10 million (Illumina, San Diego, CA).

RNA-seq analysis was carried out using Bowtie (19) and Tophat2 (20). RNA-seq BAM files generated using the Bowtie-Tophat2 pipeline were analyzed for the expression of known and unknown genes/transcripts using the Cufflinks2 pipeline (21) and included removal of reads that did not map uniquely to the mm9 ENSEMBL genome or ENSEMBL-annotated genes. Workflows included filtering to remove duplicate reads, and those with post-aligned read metrics mapping quality below 40. Our samples showed normal 3′/5′ read distribution ratios as compared to hundreds of other samples run in the CCHMC genomics core. Transcript/isoform and gene summarized expression tables were filtered to identify entities whose expression was at least 5 FPKM (fragment per kilobase of exon per million fragments mapped, Cufflinks) or 5 RPKM (reads per kilobase per million reads mapped, GeneSpring) in at least one sample. Differentially expressed gene signatures were identified using Audic Claverie tests ($P < 0.05$) and Students t test (FDR<0.05) followed by a two -fold change requirement. Gene Ontology and other enrichment and biological network analysis was carried out using ToppGene (http://toppgene.cchmc.org) (22), and ToppCluster (http://toppcluster.cchmc.org) (23). ToppCluster output of xgmml data files were network-analyzed in Cytoscape yielding both similar and complementary results as compared to the Toppfun functional enrichment analysis.

PCR and sequencing of Pkhd1 exons and intron35

For different exons of *Pkhd1*, primer pairs were designed using Primer3 (http://biotools.umassmed.edu/bioapps/primer3_www.cgi) to amplify representative exon sequences in *Pkhd1* using genomic DNA as template. PCR primer sequences are detailed in supplemental Table 3.

Primer N7_forward primer and Primer 3_reverse primer were used with PrimerStar GXL DNA Polymerase (Clontech Laboratories, Inc., CA) for long-range PCR to discover the inserted DNA fragment in *Pkhd1* intron 35 in NOD.*Abd3*. Long-range PCR products from NOD and NOD.*Abd3* were then sent for Next-Generation Sequencing at Cincinnati Children's Hospital Medical Center DNA Sequencing and Genotyping Core.

Statistical analysis

GraphPad Prism 6 (GraphPad Software, San Diego, CA) software package was used to perform unpaired, two-tailed Student t test for comparison of the expression level of genes, as well as Mann–Whitney U test to estimate significance levels of histology scores and clinical scores.

Results

A region on chromosome 1 is necessary for spontaneous autoimmune cholangitis in NOD congenic mice

We previously published that NOD.c3c4 and NOD.ABD mice, with B6/B10 genetic regions on chromosomes 3 and 4 placed on the NOD background, develop a genetically determined, spontaneous, autoimmune cholangitis; however the causative genetic regions were not clear (8-10). Further analysis of these strains by a 5K SNP chip analysis revealed a region of B6/B10-derived DNA on chromosome 1 in the NOD.c3c4 and NOD.ABD strains (Supplemental Table 1) (10). To assess the significance of this region we developed, from the NOD.ABD strain, a novel congenic mouse which had the chromosome 1 region but lacked the chromosome 3 and 4 regions ("Line 7825" in Fig 1A). This chromosome 1 congenic mouse has highly penetrant autoimmune biliary disease identical in kinetics, penetrance and phenotype to the previously published NOD.c3c4 strain. Common bile duct (CBD) dilation score (which we previously published as a sensitive marker of ABD in this strain (8)) at 120 days is identical between strain 7825 and NOD.c3c4 (strain 1112) (Fig 1B) as are liver and histology scores (not shown). We therefore designated the chromosome 1 region as "*Abd3*" (chromosome 3 and 4 regions previously described in NOD.ABD (10) were termed *Abd2* and *Abd1*, respectively).

To test if the *Abd3* region is fully recessive and is the only segregating genetic region contributing to the ABD phenotype in line 7825, we examined (line 7825 × NOD) F2 mice. Thirty-four F2 mice were scored at 120 days of age in a blinded manner for CBD and liver disease and genotyped at *Abd3*. All mice genotyped as homozygous for the NOD allele at *Abd3* (N=6) had clinically normal livers and common bile ducts, whereas all mice genotyped as homozygous for the B6/B10 allele at *Abd3* (N=10) had macroscopic disease evident in both liver and bile duct (Fig 1C). All mice genotyped as heterozygous at *Abd3* (N=18) were also phenotypically normal. This confirmed that ABD caused by the B6/B10-derived chromosome 1 region is recessive and that the chromosome 1 region is sufficient to cause disease in the context of the NOD genetic background; no other gene influencing ABD to a detectable degree is segregating outside the *Abd3* region. The effect of the chromosome 1 region on the development of autoimmune diabetes was also examined, and the frequency of diabetes in line 7825 was equivalent to that observed in the NOD parental strain, indicating that *Abd3* had no effect on T1D (Supplemental Figure 1).

To refine the *Abd3* region and aid in discovery of the causal gene, several additional congenic strains were developed by screening for recombination events in the congenic segment present in line 7825 (Fig 2A). Line 8706 has the smallest congenic interval, a maximal size of 1.0003 Mb (proximal boundary defined by rs13475762 and the distal

boundary by rs32040516); we designated this strain as "NOD.*Abd3*". Like strain 7825, NOD.*Abd3* mice developed liver histological abnormalities (lymphocytic infiltrates and biliary ductule epithelial hyperplasia) identical in appearance and kinetics to NOD.c3c4 mice (9) (Fig 2B). (NOD.*Abd3* × NOD) F1 mice lacked clinical disease and had no liver histological abnormalities compared to NOD.*Abd3* mice (Fig 2C); clearly demonstrating that *Abd3* mediates a recessive trait even at a microscopic level.

There are only a few genes in the 1 Mb *Abd3* region, including two microRNAs (miR-30a and miR-30c-2), Opioid growth factor receptor like 1 (*Ogfrl1*), a predicted gene with unknown function (Gm6420) and partial sequence of Beta-1,3-Glucuronyltransferase 2 (*B3gat2*) (Fig 2D). However, none of these genes showed significant expression differences in target tissue or CD8 T cells isolated from NOD.*Abd3* compared to NOD mice (data not shown). A comparison of the NOD and B6/B10 sequence also did not reveal any functional polymorphisms such as amino acid changing SNPs or SNPs affecting splice sites (data not shown). Notably, strains developed from proximal recombination events (lines 8727 and 8730, Fig 2A) did not develop ABD. This led us to consider the possibility that a proximal gene outside, but closely linked to, the congenic interval could be mutated and that the congenic interval was simply tagging the mutation due linkage disequilibrium.

Bile duct abnormality in NOD.Abd3 associated with aberrant expression of Pkhd1

All recombinant strains that did not develop disease had recombination events removing the proximal portion of the congenic region present in line 7825 (Fig 2A, lines 8727 and 8730), suggesting there could be a genetic mutation proximal to the *Abd3* region that was causing disease (since a recombination event removing the proximal portion of the 7825 congenic region would also replace a large portion of the DNA upstream of the congenic region with NOD DNA derived from the backcross partner). To assess this, we performed RNA-seq analysis of CBD from NOD.*Abd3* and NOD mice. We then compared the RNA-seq reads from NOD and NOD.*Abd3* CBDs focusing on 0-24 Mb (ending at the proximal border of the *Abd3* region) on chromosome 1, and found a single major genetic difference between these strains: Polycystic Kidney and Hepatic Disease 1 (*Pkhd1*) was aberrantly expressed in NOD.*Abd3* compared to NOD CBD samples (Fig 3). *Pkhd1* is located ~2.5 Mb upstream from the proximal border of the *Abd3* congenic region. In both human and murine models, *Pkhd1* mutations mediating biliary-hepatic disease (in absence of renal pathology) produce biliary duct-proliferation abnormalities similar to NOD.*Abd3* (but largely lacking significant cholangitis/inflammation)(24-27). RNA-seq-reads aligned to the reference genome showed that NOD.*Abd3* CBD lacked expression of exon 36 to exon 67 of *Pkhd1* compared to NOD controls (Fig 3A). Moreover, the read-density aligned to each exon of *Pkhd1* indicated that the expression level of exons 1-35 of *Pkhd1* in NOD.*Abd3* CBD at 2 weeks of age is higher than that in NOD CBD; in contrast, the read-density of all 67 *Pkhd1* exons in NOD was relatively constant (Fig 3B).

To rule out the possibility that truncated expression of *Pkhd1* was due to genomic DNA deletion of exons 36-67, we designed primers to amplify genomic DNA for proximal and distal exons before and after the observed transcript cutoff site at exon35-exon36). PCR showed product bands for all representative exons in NOD.*Abd3* comparable to NOD and

B6 (Fig 3C), clearly demonstrating that missing expression of *Pkhd1* exons 36 to 67 in NOD.*Abd3* was not caused by a genomic DNA deletion event. We then tested *Pkhd1* expression level using qRT-PCR. Expression of exons 15/16 in CBD from 2-week-old NOD.*Abd3* mice was nearly two times of that in NOD and B6 and the expression of exons 35/36 and 60/61 is dramatically diminished (Fig 3D), consistent with the RNA-seq results (Fig 3B). There was no significant difference in expression of these exons between NOD and B6 (Fig 3D), and the expression level within either NOD or B6 was relatively consistent (data not shown). Given these results we heretofore defined "*Abd3*" as including both the B6 genetic region and *Pkhd1*, as shown in figures 1A and 2A.

Abd3-mediated clinical autoimmune biliary disease requires the NOD genetic background but not the NOD MHC region

To examine the influence of non-MHC NOD genes on ABD, we crossed NOD.*Abd3* and B6 mice and intercrossed the resulting F1 mice. This F2 generation allows for the examination of mice homozygous for the *Abd3* region but on average having 50% NOD and 50% B6 genetic contributions to the remainder of the genome. To reduce the proportion of NOD-derived genes even further, F1 mice were backcrossed twice to B6 mice with breeders each generation selected to retain the disease-associated *Abd3* region and then intercrossed to produce BC2i mice having on average only 12.5% NOD-derived alleles. The pathological CBD enlargement and anatomically visible liver abnormalities seen in *Abd3* homozygous mice are greatly reduced and absent, respectively, in F2 and BC2i offspring that are homozygous at *Abd3* but with a reduced NOD background (Fig 4A and B). Therefore progressively reducing NOD genetic background and increasing B6 genetic background ameliorates clinical manifestations of ABD in *Abd3* homozygous animals, strongly emphasizing the importance of the NOD genetic background for the presence of clinical ABD. Notably, since clinical disease is present in a substantial proportion of the F2 mice homozygous for *Abd3*, NOD and B6 alleles contributing to disease penetrance could be mapped in future studies using a large cohort of such mice.

We performed histological analysis of the same F2 and BC2i crosses. Mice lacking the *Abd3* allele, or heterozygous for the region in the F2 and BC2i cohorts, had no histological lesions, whereas homozygous animals had reduced histology scores for duct proliferation and leukocytic infiltration compared to NOD.*Abd3* mice (Fig 4C and D). Notably, histological disease was not different between F2 and BC2i mice (Fig 4C, D), in contrast to the clinical manifestations of disease (Fig 4A, B). The fact that histology scores were similar between F2 and BC2i *Abd3* homozygous mice suggests that the B6 immune system does respond, albeit less aggressively, to the aberrant regulation of *Pkhd1*. In other words, the NOD genetic background appears not to be necessary for initiation of disease (histological lesions) but is necessary for clinical progression of disease.

The development of autoimmune diabetes in NOD mice is dependent on having at least one copy of the NOD MHC as well as a large number of other NOD background genes (28). To understand the interaction between the *Abd3* region and the NOD MHC in the context of the NOD background on the development of autoimmune biliary disease, we constructed NOD.$H2^b$ *Abd3* mice. NOD.$H2^b$ *Abd3* mice had a small but statistically significant decrease

in CBD score, but their liver score (Fig 4F) and histological severity of ABD (not shown, n=9 NOD.*Abd3* and n=24 NOD.$H2^b$*Abd3*, age 120d) were not significantly different from NOD.*Abd3* mice. This suggests that unlike type 1 diabetes in the NOD model, biliary disease was not dependent on the presence of the NOD MHC.

Early cholangiocyte damage response and abnormal immune activation in NOD.Abd3 common bile duct

In the NOD mouse, islet inflammation begins as early as 3 weeks (28) and is associated with developmental processes of the pancreatic islets. We examined the CBD of two-week-old mice and found disrupted biliary epithelial architecture in NOD.*Abd3* compared to the smooth lumen in the CBD from NOD and NOD.c3c4-*scid* mice (Fig 4E). In the liver, no significant histological difference was observed between NOD.*Abd3* and NOD control at this very early time point (not shown). These findings are consistent with our previously published results showing that hepatic inflammation was not detectable until ~8 weeks in NOD.ABD mice, and that NOD.c3c4-*scid* mice had minimal hepatic disease (8, 14). To further understand the striking difference between NOD and NOD.*Abd3* CBD architecture at 2 weeks, we performed RNA-seq on CBD from 2-week-old mice. 255 genes were significantly differentially expressed between the strains (Fig 5A). Cluster enrichment network analysis of these 255 genes based on biological processes, molecular functions, mouse knockout phenotypes and biological pathways showed that many of the genes upregulated in 2-week-old NOD.*Abd3* CBD were extensively involved in cholangiocyte injury (reflecting the tissue target cell in ABD) whereas genes involved in the immune response (both adaptive and innate) were downregulated in NOD.*Abd3* CBD (Fig 5B). Biological-process enrichment analysis shows that many of the upregulated genes in NOD.*Abd3* are involved in epithelial cell differentiation, morphology and morphogenesis (all genes associated with these processes were upregulated), while the downregulated genes are largely involved in abnormal inflammatory response/inflammation, leukocyte transendothelial migration, hepatobiliary system and gland physiology, and cellular secretion (all genes associated with these processes were downregulated) (Table one). A few processes involved both upregulated and downregulated genes, including cell adhesion and epithelial cell proliferation (Table one). These results establish that a very early tissue abnormality interacting with an abnormal immune response drives the development of NOD.*Abd3* biliary disease.

Bone marrow chimera studies demonstrate that expression of Abd3 in both target tissue and immune cells is necessary for disease

We next dissected the level at which the NOD background was acting in the autoimmune process. We had previously shown that NOD.ABD splenocytes or CD8 T cells could not transfer disease into NOD.*scid* mice, and conversely that NOD splenocytes or CD8 cells could not transfer disease into NOD.c3c4-*scid* mice. These results suggested that the *Abd3* locus acted on both the target tissue and the immune system. An alternate explanation, however, was that the NOD CD8 T cell repertoire has the potential to cause ABD, but that the disease-mediating T cell clones were not expanded since they were never exposed to their tissue autoantigen (i.e. NOD mice lack abnormal BECs). To distinguish between these possibilities we performed bone marrow chimera studies. NOD.*Abd3* irradiated recipients

were reconstituted with either NOD or NOD.*Abd3* bone marrow, and conversely, NOD recipients were reconstituted with NOD.*Abd3* bone marrow. The results clearly reproduced the transfer study findings: the recipients must express NOD.*Abd3* in biliary tissue to develop disease. NOD.*Abd3*→NOD recipients had no clinical abnormality in CBD or liver (Fig 6A, bars 7 and 8, significantly different from NOD.*Abd3*→NOD.*Abd3* recipients) and no duct epithelial hyperplasia and minimal lymphocytic infiltrates (Fig 6B, bars 7 and 8, significantly different from NOD.*Abd3*→NOD.*Abd3* recipients). In addition, NOD BM did not cause significant disease in NOD.*Abd3* recipients—both the clinical gross liver score and histological duct epithelial hyperplasia score at 120 days post-BM transplant were significantly less than NOD.*Abd3*→NOD.*Abd3* recipients (Fig 6A and B). NOD.*Abd3* recipients already had some disease at the time of irradiation (Fig 6A and B; bars 1 and 2). In the NOD.*Abd3* →NOD.*Abd3* transfer the NOD.*Abd3* bone marrow repopulated the mouse and caused the disease to progress. In the NOD→ NOD.*Abd3* mice, the NOD bone marrow not only did not accelerate the disease, but actually reduced the histological score compared to 10-week-old NOD.*Abd3* mice (Fig 6B, bars 1 and 2 compared to bars 5 and 6). Therefore, there is clearly a difference in the ability of the hematopoietic system to cause disease between the NOD and NOD.*Abd3* strains; the *Abd3* mutant *Pkhd1* allele must be expressed in both the hematopoietic system and target tissue in order for autoimmune biliary disease to develop.

Although, to our knowledge, the expression of *Pkhd1* in immune cells has never been reported previously, the Ensembl database shows that RNA-seq reads from spleen are aligned to *Pkhd1* (29). We hypothesized that deficient exon expression pattern of *Pkhd1* could be detected not only in CBD, the target tissue, but also in immune cells, explaining why both systems were necessary for ABD. However, we were unable to detect the *Pkhd1* expression in unactivated splenocytes, intrahepatic immune cells (IHC), or MACS-sorted CD4 or CD8 T cells from spleen and liver using exons 15/16, 35/36 and 60/61 (data not shown).

Details of the Pkhd1 genetic mutation in NOD.Abd3 and potential mechanism of truncated transcription

Pkhd1 is ~2.5 Mb upstream from the *Abd3* allele (Figure 7A). The RNA-seq data as well as the qRTPCR result revealed a novel loss of *Pkhd1* transcription after exon35, and we sought to understand how this transcription deregulation occurs in NOD.*Abd3*. The alignment of the RNA-seq reads from 2-week-old NOD.*Abd3* CBD and NOD CBD identified a unique, transcribed intronic region immediately after exon 35 (the second longest *Pkhd1* intron) in NOD.*Abd3* but not in NOD (Fig 7B). We found no mutations at the splice donor site (“GT”) after exon35 or splice acceptor site (“AG”) before the start of exon 36. On the other hand, there were multiple microsatellite repeats in the uniquely transcribed intron region and poly(A) signal (AAUAAA), which suggested that it could be a 3′ UTR-like region (30) in *Pkhd1*.

To evaluate further the unique 3′ UTR-like region in intron 35 of NOD.*Abd3 Pkhd1*, we designed 3 primer pairs (Primers 1-3 in Table 2, Supplemental Table 3) to perform tiled PCR starting from the end of the 3′ UTR-like region in intron 35 towards exon 35 (Fig 8A). The

first two pairs of tiled PCR primers at the end of the novel 3′ UTR-like region of intron 35 amplified in NOD but not in NOD.*Abd3* (Fig 8B, Table 2). We then designed 7 primer pairs (every 5kb) from exon 36 towards the end of the novel 3′ UTR like region in intron 35 (N1-N7, Table 2, Supplemental Table 3). Each of these primer pairs amplified in both NOD and NOD.*Abd3* (Fig 7C). Lastly, using the forward primer of primer pair N7 and the reverse primer of primer pair 3 (Table 2, Fig 8A) we found a PCR product size in NOD was ~3kb (similar to reference target sequence). In striking contrast, the PCR product size in NOD.*Abd3* was ~9kb (Fig 8D). Therefore, the mutation within *Pkhd1* was a DNA insertion of about 6 kb.

Using Next-Generation Sequencing technology, we sequenced the PCR products through de novo reads-assembly. The assembled PCR product sequence of NOD could be fully aligned with the reference genome while only part of the three nodes of assembly sequence of NOD.*Abd3* matched with NOD sequence. The node-2 assembled sequence in NOD.*Abd3 Pkhd1* intron 35 was analyzed in RepeatMasker and had 99.73% identity with long terminal repeat (LTR) elements of four class II endogenous retroviruses (ERV) (Fig 8E).

Given these results of genetic characterization of *Pkhd1* in NOD.*Abd3*, we propose the following potential mechanism: the 6kb LTR ERV DNA insertion in intron 35 of NOD.*Abd3 Pkhd1* disrupts normal recognition of splicing sites in this intron and forces the exposure of an alternative polyadenylation site within the intron, thus giving rise to a novel shortened transcript which ends after exon 35 (Fig 8F). Given that qRT-PCR and RNA-seq show an upregulation of the first 35 exons of *Pkhd1* in NOD.*Abd3* CBD, this alternative polyadenylation (APA) site must predominate over the normal polyadenylation site (after exon 67) in NOD.*Abd3*.

In summary, we have shown that ABD in NOD congenic mouse strains is associated with a novel *Pkhd1* mutation. Uniquely, on the NOD background, this mutation results in an autoimmune disease that depends on expression of mutated *Pkhd1* in both the target tissue and hematopoetic system. Early abnormalities in cholangiocyte morphology and development are accompanied by dysregulation of the immune system, resulting in a genetically controlled autoimmune disease.

Discussion

Here we prove conclusively that NOD ABD is caused by a recessively acting region on chromosome 1. This region, designated "*Abd3*", is necessary and sufficient for ABD when on the NOD background. The only genetic difference we found in the *Abd3* region of diseased NOD.*Abd3* compared to NOD mice was aberrant expression of *Pkhd1. Pkhd1* is a large gene with 67 exons (4059 amino acids) encoding fibrocystin, a membrane-associated receptor-like protein with a single transmembrane domain, a small intracellular domain, and a large extracellular domain containing multiple repeats of IPT (immunoglobulin–like plexin-transcription) factor domains and two G8 domains (predicted to contain 10 beta strands and an alpha helix) (31, 32). We anticipate that the mutated *Pkhd1* protein in NOD.*Abd3* mice, if it is expressed, has lost the G8 domains as well as the transmembrane and intracellular domains. Fibrocystin has domains that are similar to those found in plexin

and hepatocyte growth factor families; these domains function in cellular adhesion and proliferation (25). *Pkhd1* is extensively alternatively spliced, and spliced differently in different cell types, but a role for alternately spliced products has not been demonstrated (33, 34). The human and mouse protein sequences share 73% identity (31, 35). During embryogenesis, fibrocystin is widely expressed in epithelial derivatives, including neural tubules, gut, pulmonary bronchi, renal cells and hepatic cells. By embryonic day 15 fibrocystin is strongly expressed in bile duct cholangiocyte cilia, and in the epithelial cells in the kidney collecting tubes (33, 36, 37). Monoclonal antibodies also detect fibrocystin in human pancreatic duct, islets, testis and adrenal gland (38).

NOD.*Abd3* mice have normal renal structure throughout life. Consistent with this, prior mouse models with engineered deletions of *Pkhd1* have no renal abnormalities. Mice with targeted deletion of *Pkhd1* exons 3, 4 or 40 had no kidney abnormality, but demonstrated intrahepatic bile duct proliferation with progressive cyst formation (similar to our model) and associated periportal fibrosis (not seen in NOD.*Abd3* mice) (24, 25, 34). *Pkhd1*^{ex4del} mice develop splenomegaly, which is also found in our model. *Pkhd1*^{ex4del} mice develop a syndrome of congenital hepatic fibrosis, and *Pkhd1*^{ex4del} cholangiocytes secrete chemokines, including CXCL 1, 2, and 12, that aberrantly recruit macrophages (39). Macrophage depletion in *Pkhd1*^{ex4del} mice decreases both fibrosis and cystic disease. The similarity of the biliary epithelial abnormalities and, in some cases, the presence of hematopoietic cell infiltrates in these other models of *Pkhd1* mutation, leads us to conclude that mutated *Pkhd1* is the primary cause of ABD in our model. Our model is unique, however, because none of the previous models were shown to involve an autoimmune response nor did they require, as far as we know, *Pkhd1* expression in hematopoietic cells.

Disease expression in other *Pkhd1* models was also apparently unaffected by the genetic background. Thus the role of genetic background in our model is also unique; we show decreased histological abnormalities (and reduced or no clinical disease depending on the amount of residual NOD genetic material remaining) when the *Pkhd1* mutation is expressed on a genetic background that is predominantly B6. Notably, however, there was no significant difference in histological disease scores between F2 and BC2i mice (Fig 4C, D), suggesting that disease initiation (manifest in histological lesions) does not require the NOD genetic background. In contrast, clinical disease (liver and CBD scores in Fig 4A, B) requires the NOD genetic background. Although outside the scope of the current study, mapping the NOD background regions required for clinical disease in conjunction with *Abd3* homozygosity would be achievable by genetic analysis of (NOD.*Abd3* × B6)F2 mice having two doses of the *Abd3* region since disease was observed to be present in a portion of these mice (Fig 4A, B). We note that introgression of genetic regions derived from B6 or B10 mice into the NOD strain that prevent type 1 diabetes, i.e. introgression of the MHC region and large segments of chromosomes 3 and 4 (9, 16), do not prevent clinical or histological ABD in the presence of *Abd3* homozygosity (Fig 4F, reference 9). This suggests that NOD genes distinct from those critical for the development of type 1 diabetes in the NOD model may be essential for the clinical manifestation of ABD.

At this point, we cannot fully explain our findings, since we have been unable to verify *Pkhd1* expression in the immune cells we have tested. It is possible that the upregulated

Pkhd1 exons 1-35 play a role in immune cells; another possibility is that mutant *Pkhd1* affects alternative splicing in an immune cell subset (eg macrophages) and that we need to use different primers to detect the immune-cell specific transcript. *Pkhd1* expression in the thymus could affect the immune repertoire. Finally, we cannot exclude that the linked B6-derived congenic region present in the NOD.*Abd3* strain plays some role in the pathogenesis of these mice. Although we have not shown any differentially expressed genes from this region, we will ultimately only be able to formally disprove a role of the 1.0 Mb B6-derived congenic segment within the *Abd3* region, in future studies, by selecting a recombination event between the congenic region and *Pkhd1* and testing the effect of the mutant *Pkhd1* gene in the absence of the congenic region (on the NOD background) on disease.

Bone marrow and splenocyte-transfer studies show that the *Abd3* allele / mutated *Pkhd1* must be expressed in both immune system and target tissue to develop cholangitis. The question remains how an alteration of a single gene (*Pkhd1*) involved in cilia function and epithelial integrity in cholangiocytes can ultimately lead to an autoimmune disease. Interestingly, the biological process-enrichment analysis of RNA-seq data from NOD.*Abd3* CBD reveals a striking pattern with the down-regulated genes extensively involved in acute immune/inflammatory response (Table 1). Many of these genes can negatively regulate the immune response, thus mediating a protective role against, for example, over-exuberant immune responses to microbial infection. For example, although there are large number of reports on its pro-inflammatory effect, *S100A9* (Table 1) also has anti-inflammatory effects though inhibition of neutrophil oxidative metabolism (40, 41) and neutrophil chemorepulsion. *Serpinc1* can induce the anti-inflammatory cytokine PGI2 from cultured human umbilical vein endothelial cells (42); *Spdef* negatively regulates TLR signaling in airway epithelial cells(43); *Vip* executes protective humoral responses against pathogens (44), and *CORO1A* is linked to inhibition of neutrophil apoptosis in chronic inflammation which is essential to resolve inflammation (45).

Downregulation of several of these genes results in increased inflammation and autoimmune disease, eg. ablation of *Syt7* in mice resulted in inflammatory myopathy (46); *C2GnT2* KO mice have decreased mucosal barrier function in the digestive tract, reduced levels of circulating IgGs and fecal IgA, and increased susceptibility to experimental colitis (47), and complement deficiency is associated with lupus (48). We speculate that the downregulation of these anti-inflammatory/regulatory genes in the innate immune system or in cholangiocytes makes it difficult to resolve inflammatory responses, which may facilitate the generation of neoantigen in the target tissue. Generation of neoantigens, in the presence of altered bile composition and abnormal duct physiology, could escalate the immune response and progression to an adaptive immune response to self-targets.

Mutation of *Pkhd1* likely results in a cholangiociliopathy with impaired primary cholangiocyte cilia. Defective cilia structure can compromise the integrated sensory/transducing functions resulting in increased cholangiocyte cAMP and decreased [Ca2+] (49), causing cholangiocyte hyperproliferation, changes in metabolic processes, abnormal cell-matrix interactions and altered fluid secretion/absorption (water and bile modification) as reflected by the gene cluster analysis (Figure 5B, Table 1). Therefore, the entire

cholangiocyte environment is changed, and the outcome of the change in one gene (*Pkhd1*) leads to both altered morphogenesis and altered immune-related responses.

The results of the bone marrow transfer studies clearly demonstrate that NOD.*Abd3* immune cells are pathogenic, while NOD immune cells are not. NOD T cells are unable to cause disease even when they develop in an $Abd3^{+}$ host with abnormal cholangiocytes. Taken together with a similar result in our transfer studies (14), this suggests that the *Pkhd1* mutation must be expressed both in the target tissue and in the hematopoietic tissue. The requirement of the NOD genetic background (which is highly disposed to autoimmunity) for disease manifestation, in contrast, supports the idea that the immune system perpetuates and enhances cholangitis in NOD.*Abd3* mice. Future studies will be directed to discover the critical immune subsets and the mechanism by which the *Pkhd1* mutation affects the immune system.

In summary, we have identified a novel mutation in *Pkhd1* as a key genetic factor causing the biliary tissue abnormality and activating the adaptive immune system in the context of NOD genetic background. Although we have clearly demonstrated that both the target tissue (cholangiocytes) and the immune system must express the *Pkhd1* mutation, we do not yet understand the role of the mutation in each system or how the systems interact. Abnormalities involving hundreds of both tissue-specific (cholangiocyte specific) and immune-origin genes are affected by 2 weeks of age, indicating a complex, orchestrated event producing this organ specific autoimmune disease. Our mouse model of spontaneously mutated *Pkhd1* is thus valuable for exploring several cholangiopathies including primary biliary cholangitis, primary sclerosing cholangitis, and polycystic hepatobiliary disease.

Supplementary Material

Refer to Web version on PubMed Central for supplementary material.

Acknowledgments

We thank Mehdi Keddache and Satwica Yerneni for their assistance with the RNA-sequencing

Financial support: This research was funded by the Biomedical Laboratory Research & Development Service of the VA Office of Research and Development, VA merit grant BX000827-01A1 (WMR). LSW and DBR were supported by Wellcome Trust Grant 107212/Z/15/Z and JDRF Grant 4-SRA-2017-473-A-N. The Wellcome Trust Center for Human Genetics is supported by a core reward from the Wellcome Trust (203141/Z/16/Z). WMR, LSW, and MEG were supported by NIH R01DK074768.

References

1. Kaplan MM, Gershwin ME. Primary biliary cirrhosis. N Engl J Med. 2005; 353:1261–1273. [PubMed: 16177252]
2. Invernizzi P, Selmi C, Gershwin ME. Update on primary biliary cirrhosis. Digestive and Liver Disease. 2010; 42:401–408. [PubMed: 20359968]
3. Eaton JE, Talwalkar JA, Lazaridis KN, Gores GJ, Lindor KD. Pathogenesis of primary sclerosing cholangitis and advances in diagnosis and management. Gastroenterology. 2013; 145:521–536. [PubMed: 23827861]
4. Mack CL. The Pathogenesis of Biliary Atresia: Evidence for a Virus-Induced Autoimmune Disease. Semin Liver Dis. 2007; 27:233–242. [PubMed: 17682970]

5. Brindley SM, Lanham AM, Karrer FM, Tucker RM, Fontenot AP, Mack CL. Cytomegalovirus-specific T-cell reactivity in biliary atresia at the time of diagnosis is associated with deficits in regulatory T cells. Hepatology. 2012; 55:1130–1138. [PubMed: 22105891]
6. Rong G, Zhong R, Lleo A, Leung PSC, Bowlus CL, Yang GX, Yang CY, Coppel RL, Ansari AA, Cuebas DA, Worman HJ, Invernizzi P, Gores GJ, Norman G, He XS, Gershwin ME. Epithelial cell specificity and apotope recognition by serum autoantibodies in primary biliary cirrhosis. Hepatology. 2011; 54:196–203. [PubMed: 21488079]
7. Shivakumar P, Sabla G, Mohanty S, McNeal M, Ward R, Stringer K, Caldwell C, Chougnet C, Bezerra JA. Effector Role of Neonatal Hepatic CD8+ Lymphocytes in Epithelial Injury and Autoimmunity in Experimental Biliary Atresia. Gastroenterology. 2007; 133:268–277. [PubMed: 17631148]
8. Irie J, Wu Y, Wicker LS, Rainbow D, Nalesnik MA, Hirsch R, Peterson LB, Leung PSC, Cheng C, Mackay IR, Gershwin ME, Ridgway WM. NOD.c3c4 congenic mice develop autoimmune biliary disease that serologically and pathogenetically models human primary biliary cirrhosis. The Journal of Experimental Medicine. 2006; 203:1209–1219. [PubMed: 16636131]
9. Koarada S, Wu Y, Fertig N, Sass DA, Nalesnik M, Todd JA, Lyons PA, Fenyk-Melody J, Rainbow DB, Wicker LS, Peterson LB, Ridgway WM. Genetic Control of Autoimmunity: Protection from Diabetes, but Spontaneous Autoimmune Biliary Disease in a Nonobese Diabetic Congenic Strain. The Journal of Immunology. 2004; 173:2315–2323. [PubMed: 15294944]
10. Yang GX, Wu Y, Tsukamoto H, Leung PS, Lian ZX, Rainbow DB, Hunter KM, Morris GA, Lyons PA, Peterson LB, Wicker LS, Gershwin ME, Ridgway WM. CD8 T cells mediate direct biliary ductule damage in nonobese diabetic autoimmune biliary disease. J Immunol. 2011; 186:1259–1267. [PubMed: 21169553]
11. Oertelt S, Lian ZX, Cheng CM, Chuang YH, Padgett KA, He XS, Ridgway WM, Ansari AA, Coppel RL, Li MO, Flavell RA, Kronenberg M, Mackay IR, Gershwin ME. Anti-Mitochondrial Antibodies and Primary Biliary Cirrhosis in TGF-β Receptor II Dominant-Negative Mice. The Journal of Immunology. 2006; 177:1655–1660. [PubMed: 16849474]
12. Shivakumar P, Campbell KM, Sabla GE, Miethke A, Tiao G, McNeal MM, Ward RL, Bezerra JA. Obstruction of extrahepatic bile ducts by lymphocytes is regulated by IFN-γ in experimental biliary atresia. The Journal of Clinical Investigation. 2004; 114:322–329. [PubMed: 15286798]
13. Torres VE. Polycystic liver disease. Contrib Nephrol. 1995; 115:44–52. [PubMed: 8585918]
14. Yang GX, Wu Y, Tsukamoto H, Leung PS, Lian ZX, Rainbow DB, Hunter KM, Morris GA, Lyons PA, Peterson LB, Wicker LS, Gershwin ME, Ridgway WM. CD8 T Cells Mediate Direct Biliary Ductule Damage in Nonobese Diabetic Autoimmune Biliary Disease. The Journal of Immunology. 2011; 186:1259–1267. [PubMed: 21169553]
15. Hamilton-Williams EE, Martinez X, Clark J, Howlett S, Hunter KM, Rainbow DB, Wen L, Shlomchik MJ, Katz JD, Beilhack GF, Wicker LS, Sherman LA. Expression of diabetes-associated genes by dendritic cells and CD4 T cells drives the loss of tolerance in nonobese diabetic mice. J Immunol. 2009; 183:1533–1541. [PubMed: 19592648]
16. Wicker LS, Appel MC, Dotta F, Pressey A, Miller BJ, DeLarato NH, Fischer PA, Boltz RC Jr, Peterson LB. Autoimmune syndromes in major histocompatibility complex (MHC) congenic strains of nonobese diabetic (NOD) mice. The NOD MHC is dominant for insulitis and cyclophosphamide-induced diabetes. J Exp Med. 1992; 176:67–77. [PubMed: 1613467]
17. Bednar KJ, Tsukamoto H, Kachapati K, Ohta S, Wu Y, Katz JD, Ascherman DP, Ridgway WM. Reversal of New-Onset Type 1 Diabetes With an Agonistic TLR4/MD-2 Monoclonal Antibody. Diabetes. 2015; 64:3614–3626. [PubMed: 26130764]
18. Fraser HI, Howlett S, Clark J, Rainbow DB, Stanford SM, Wu DJ, Hsieh YW, Maine CJ, Christensen M, Kuchroo V, Sherman LA, Podolin PL, Todd JA, Steward CA, Peterson LB, Bottini N, Wicker LS. Ptpn22 and Cd2 Variations Are Associated with Altered Protein Expression and Susceptibility to Type 1 Diabetes in Nonobese Diabetic Mice. J Immunol. 2015; 195:4841–4852. [PubMed: 26438525]
19. Langmead B, Trapnell C, Pop M, Salzberg S. Ultrafast and memory-efficient alignment of short DNA sequences to the human genome. Genome Biol. 2009; 10:1–10.

20. Kim D, Pertea G, Trapnell C, Pimentel H, Kelley R, Salzberg S. TopHat2: accurate alignment of transcriptomes in the presence of insertions, deletions and gene fusions. Genome Biol. 2013; 14:R36. [PubMed: 23618408]
21. Trapnell C, Roberts A, Goff L, Pertea G, Kim D, Kelley DR, Pimentel H, Salzberg SL, Rinn JL, Pachter L. Differential gene and transcript expression analysis of RNA-seq experiments with TopHat and Cufflinks. Nat Protocols. 2012; 7:562–578. [PubMed: 22383036]
22. Chen J, Xu H, Aronow B, Jegga A. Improved human disease candidate gene prioritization using mouse phenotype. BMC Bioinformatics. 2007; 8:392. [PubMed: 17939863]
23. Kaimal V, Bardes EE, Tabar SC, Jegga AG, Aronow BJ. ToppCluster: a multiple gene list feature analyzer for comparative enrichment clustering and network-based dissection of biological systems. Nucleic Acids Research. 2010; 38:W96–W102. [PubMed: 20484371]
24. Gallagher AR, Esquivel EL, Briere TS, Tian X, Mitobe M, Menezes LF, Markowitz GS, Jain D, Onuchic LF, Somlo S. Biliary and Pancreatic Dysgenesis in Mice Harboring a Mutation in Pkhd1. The American Journal of Pathology. 2008; 172:417–429. [PubMed: 18202188]
25. Moser M, Matthiesen S, Kirfel J, Schorle H, Bergmann C, Senderek J, Rudnik-Schöneborn S, Zerres K, Buettner R. A mouse model for cystic biliary dysgenesis in autosomal recessive polycystic kidney disease (ARPKD). Hepatology. 2005; 41:1113–1121. [PubMed: 15830394]
26. Woollard JR, Punyashtiti R, Richardson S, Masyuk TV, Whelan S, Huang BQ, Lager DJ, vanDeursen J, Torres VE, Gattone VH, LaRusso NF, Harris PC, Ward CJ. A mouse model of autosomal recessive polycystic kidney disease with biliary duct and proximal tubule dilatation. Kidney Int. 2007; 72:328–336. [PubMed: 17519956]
27. Williams S, Cobo-Stark P, James L, Somlo S, Igarashi P. Kidney cysts, pancreatic cysts, and biliary disease in a mouse model of autosomal recessive polycystic kidney disease. Pediatr Nephrol. 2008; 23:733–741. [PubMed: 18286309]
28. Bouma G, Coppens JMC, Mourits S, Nikolic T, Sozzani S, Drexhage HA, Versnel MA. Evidence for an enhanced adhesion of DC to fibronectin and a role of CCL19 and CCL21 in the accumulation of DC around the pre-diabetic islets in NOD mice. European Journal of Immunology. 2005; 35:2386–2396. [PubMed: 16047341]
29. Flicek P, Amode MR, Barrell D, Beal K, Billis K, Brent S, Carvalho-Silva D, Clapham P, Coates G, Fitzgerald S, Gil L, Girón CG, Gordon L, Hourlier T, Hunt S, Johnson N, Juettemann T, Kähäri AK, Keenan S, Kulesha E, Martin FJ, Maurel T, McLaren WM, Murphy DN, Nag R, Overduin B, Pignatelli M, Pritchard B, Pritchard E, Riat HS, Ruffier M, Sheppard D, Taylor K, Thormann A, Trevanion SJ, Vullo A, Wilder SP, Wilson M, Zadissa A, Aken BL, Birney E, Cunningham F, Harrow J, Herrero J, Hubbard TJP, Kinsella R, Muffato M, Parker A, Spudich G, Yates A, Zerbino DR, Searle SMJ. Ensembl 2014. Nucleic Acids Research. 2014; 42:D749–D755. [PubMed: 24316576]
30. Mignone F, Gissi C, Liuni S, Pesole G. Untranslated regions of mRNAs. Genome Biol. 2002; 3 reviews0004.0001-reviews0004.0010.
31. Onuchic LF, Furu L, Nagasawa Y, Hou X, Eggermann T, Ren Z, Bergmann C, Senderek J, Esquivel E, Zeltner R, Rudnik-Schöneborn S, Mrug M, Sweeney W, Avner ED, Zerres K, Guay-Woodford LM, Somlo S, Germino GG. PKHD1, the Polycystic Kidney and Hepatic Disease 1 Gene, Encodes a Novel Large Protein Containing Multiple Immunoglobulin-Like Plexin-Transcription–Factor Domains and Parallel Beta-Helix 1 Repeats. The American Journal of Human Genetics. 2002; 70:1305–1317. [PubMed: 11898128]
32. Xiong H, Chen Y, Yi Y, Tsuchiya K, Moeckel G, Cheung J, Liang D, Tham K, Xu X, Chen XZ, Pei Y, Zhao ZJ, Wu G. A Novel Gene Encoding a TIG Multiple Domain Protein Is a Positional Candidate for Autosomal Recessive Polycystic Kidney Disease. Genomics. 2002; 80:96–104. [PubMed: 12079288]
33. Nagasawa Y, Matthiesen S, Onuchic LF, Hou X, Bergmann C, Esquivel E, Senderek J, Ren Z, Zeltner R, Furu L, Avner E, Moser M, Somlo S, Guay-Woodford L, Buttner R, Zerres K, Germino GG. Identification and characterization of Pkhd1, the mouse orthologue of the human ARPKD gene. J Am Soc Nephrol. 2002; 13:2246–2258. [PubMed: 12191969]
34. Bakeberg JL, Tammachote R, Woollard JR, Hogan MC, Tuan HF, Li M, van Deursen JM, Wu Y, Huang BQ, Torres VE, Harris PC, Ward CJ. Epitope-tagged Pkhd1 tracks the processing,

secretion, and localization of fibrocystin. J Am Soc Nephrol. 2011; 22:2266–2277. [PubMed: 22021705]

35. Ward CJ, Hogan MC, Rossetti S, Walker D, Sneddon T, Wang X, Kubly V, Cunningham JM, Bacallao R, Ishibashi M, Milliner DS, Torres VE, Harris PC. The gene mutated in autosomal recessive polycystic kidney disease encodes a large, receptor-like protein. Nat Genet. 2002; 30:259–269. [PubMed: 11919560]
36. Masyuk TV, Huang BQ, Ward CJ, Masyuk AI, Yuan D, Splinter PL, Punyashthiti R, Ritman EL, Torres VE, Harris PC, Larusso NF. Defects in cholangiocyte fibrocystin expression and ciliary structure in the PCK rat1. Gastroenterology. 2003; 125:1303–1310. [PubMed: 14598246]
37. Zhang MZ, Mai W, Li C, Cho Sy, Hao C, Moeckel G, Zhao R, Kim I, Wang J, Xiong H, Wang H, Sato Y, Wu Y, Nakanuma Y, Lilova M, Pei Y, Harris RC, Li S, Coffey RJ, Sun L, Wu D, Chen XZ, Breyer MD, Zhao ZJ, McKanna JA, Wu G. PKHD1 protein encoded by the gene for autosomal recessive polycystic kidney disease associates with basal bodies and primary cilia in renal epithelial cells. Proceedings of the National Academy of Sciences of the United States of America. 2004; 101:2311–2316. [PubMed: 14983006]
38. Ward CJ, Yuan D, Masyuk TV, Wang X, Punyashthiti R, Whelan S, Bacallao R, Torra R, LaRusso NF, Torres VE, Harris PC. Cellular and subcellular localization of the ARPKD protein; fibrocystin is expressed on primary cilia. Human Molecular Genetics. 2003; 12:2703–2710. [PubMed: 12925574]
39. Locatelli L, Cadamuro M, Spirli C, Fiorotto R, Lecchi S, Morell CM, Popov Y, Scirpo R, De Matteis M, Amenduni M, Pietrobattista A, Torre G, Schuppan D, Fabris L, Strazzabosco M. Macrophage recruitment by fibrocystin-defective biliary epithelial cells promotes portal fibrosis in congenital hepatic fibrosis. Hepatology. 2016; 63:965–982. [PubMed: 26645994]
40. Sroussi HY, Lu Y, Zhang QL, Villines D, Marucha PT. S100A8 and S100A9 inhibit neutrophil oxidative metabolism in-vitro: Involvement of adenosine metabolites. Free Radical Research. 2010; 44:389–396. [PubMed: 20166886]
41. Sroussi HY, Lu Y, Villines D, Sun Y. The down regulation of neutrophil oxidative metabolism by S100A8 and S100A9: Implication of the protease-activated receptor-2. Molecular Immunology. 2012; 50:42–48. [PubMed: 22204866]
42. Horie S, Ishii H, Kazama M. Heparin-like glycosaminoglycan is a receptor for antithrombin III-dependent but not for thrombin-dependent prostacyclin production in human endothelial cells. Thrombosis research. 1990; 59:895–904. [PubMed: 2175954]
43. Korfhagen TR, Kitzmiller J, Chen G, Sridharan A, Haitchi HM, Hegde RS, Divanovic S, Karp CL, Whitsett JA. SAM-pointed domain ETS factor mediates epithelial cell–intrinsic innate immune signaling during airway mucous metaplasia. Proceedings of the National Academy of Sciences. 2012; 109:16630–16635.
44. El Karim IA, Linden GJ, Orr DF, Lundy FT. Antimicrobial activity of neuropeptides against a range of micro-organisms from skin, oral, respiratory and gastrointestinal tract sites. Journal of Neuroimmunology. 2008; 200:11–16. [PubMed: 18603306]
45. Moriceau S, Kantari C, Mocek J, Davezac N, Gabillet J, Guerrera IC, Brouillard F, Tondelier D, Sermet-Gaudelus I, Danel C, Lenoir G, Daniel S, Edelman A, Witko-Sarsat V. Coronin-1 Is Associated with Neutrophil Survival and Is Cleaved during Apoptosis: Potential Implication in Neutrophils from Cystic Fibrosis Patients. The Journal of Immunology. 2009; 182:7254–7263. [PubMed: 19454722]
46. Chakrabarti S, Kobayashi KS, Flavell RA, Marks CB, Miyake K, Liston DR, Fowler KT, Gorelick FS, Andrews NW. Impaired membrane resealing and autoimmune myositis in synaptotagmin VII–deficient mice. The Journal of Cell Biology. 2003; 162:543–549. [PubMed: 12925704]
47. Stone EL, Lee SH, Ismail MN, Fukuda M. Characterization of mice with targeted deletion of the gene encoding core 2 beta1,6-N-acetylglucosaminyltransferase-2. Methods in enzymology. 2010; 479:155–172. [PubMed: 20816165]
48. Manderson AP, Botto M, Walport MJ. The Role of Complement in the Development of Systemic Lupus Erythematosus. Annual Review of Immunology. 2004; 22:431–456.
49. Masyuk AI, Masyuk TV, LaRusso NF. CHOLANGIOCYTE PRIMARY CILIA IN LIVER HEALTH AND DISEASE. Developmental dynamics : an official publication of the American Association of Anatomists. 2008; 237:2007–2012. [PubMed: 18407555]

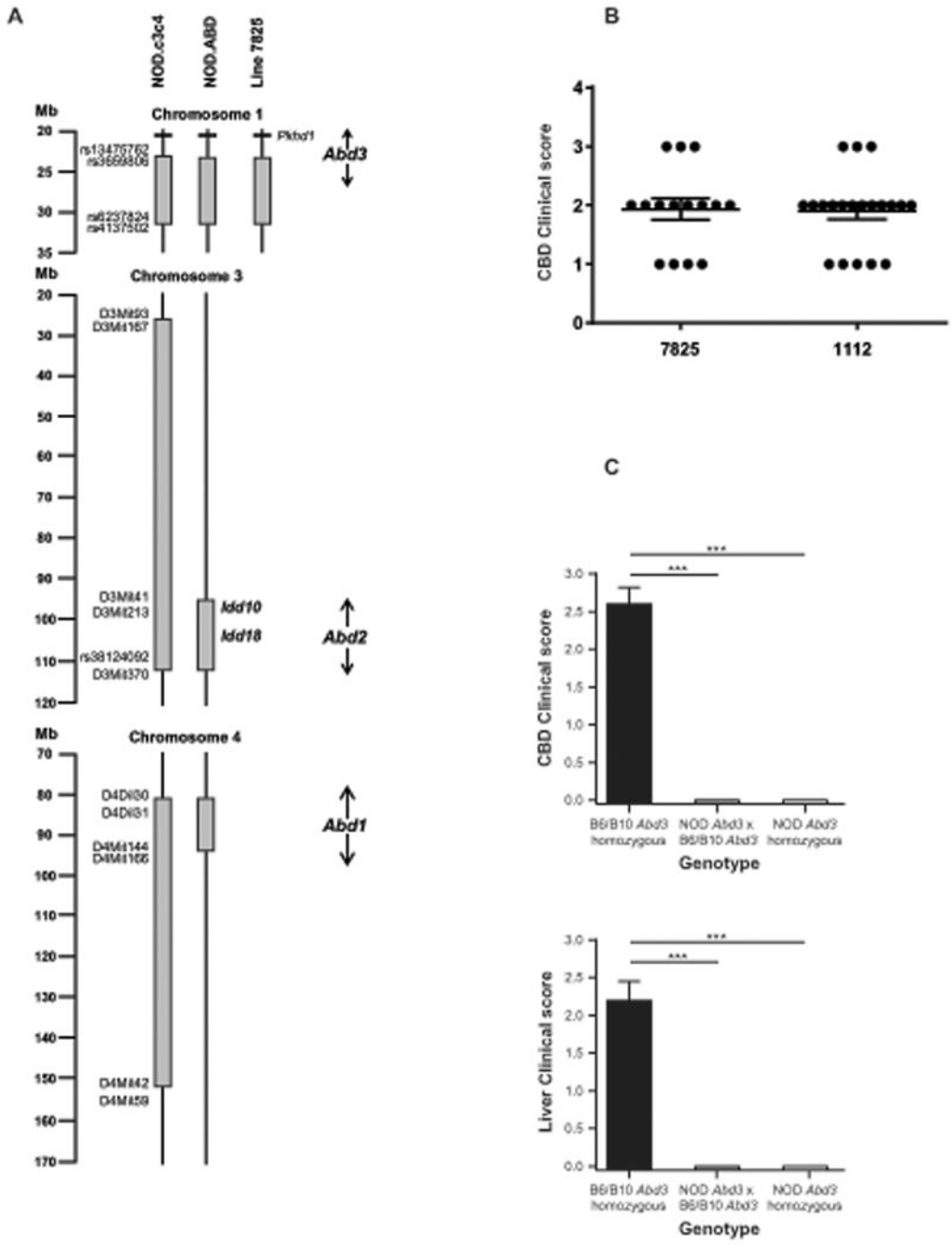

Figure 1. Autoimmune biliary disease in NOD mice is controlled by a single recessive allele on chromosome 1

A. The NOD.c3c4 strain (8, 9), NOD.ABD strain (10), and the newly developed line 7825 all develop ABD and share a non-NOD congenic region (derived from the B6.PL or B10 strain) on chromosome 1 that includes *Pkhd1*, designated "*Abd3*". The 7825 strain lacks the *Abd1* and *Abd2* regions on chromosomes 4 and 3, respectively. **B.** No difference in NOD.c3c4 vs. strain 7825 liver disease kinetics or penetrance. NOD.c3c4 (strain 1112) (n=20) and strain 7825 mice (n=15) were aged to 120 days then assessed for CBD score (see

methods). **C.** *Abd3* region homozygosity required for ABD; mice lacking two copies of 7825-derived *Abd3* do not develop any biliary disease. Anatomical liver/biliary scores (CBD score and liver score, see methods) of (7825 × NOD) F2 mice genotyped as B6/B10 *Abd3* homozygous (n = 10), NOD *Abd3* homozygous (n = 6) and NOD *Abd3* × B6/B10 *Abd3* heterozygous (n=18) using markers for the chromosome 1 congenic region (see methods). Mann-Whitney U test was performed for statistical significance. ***$P < 0.001$. Error bars displayed as SEM.

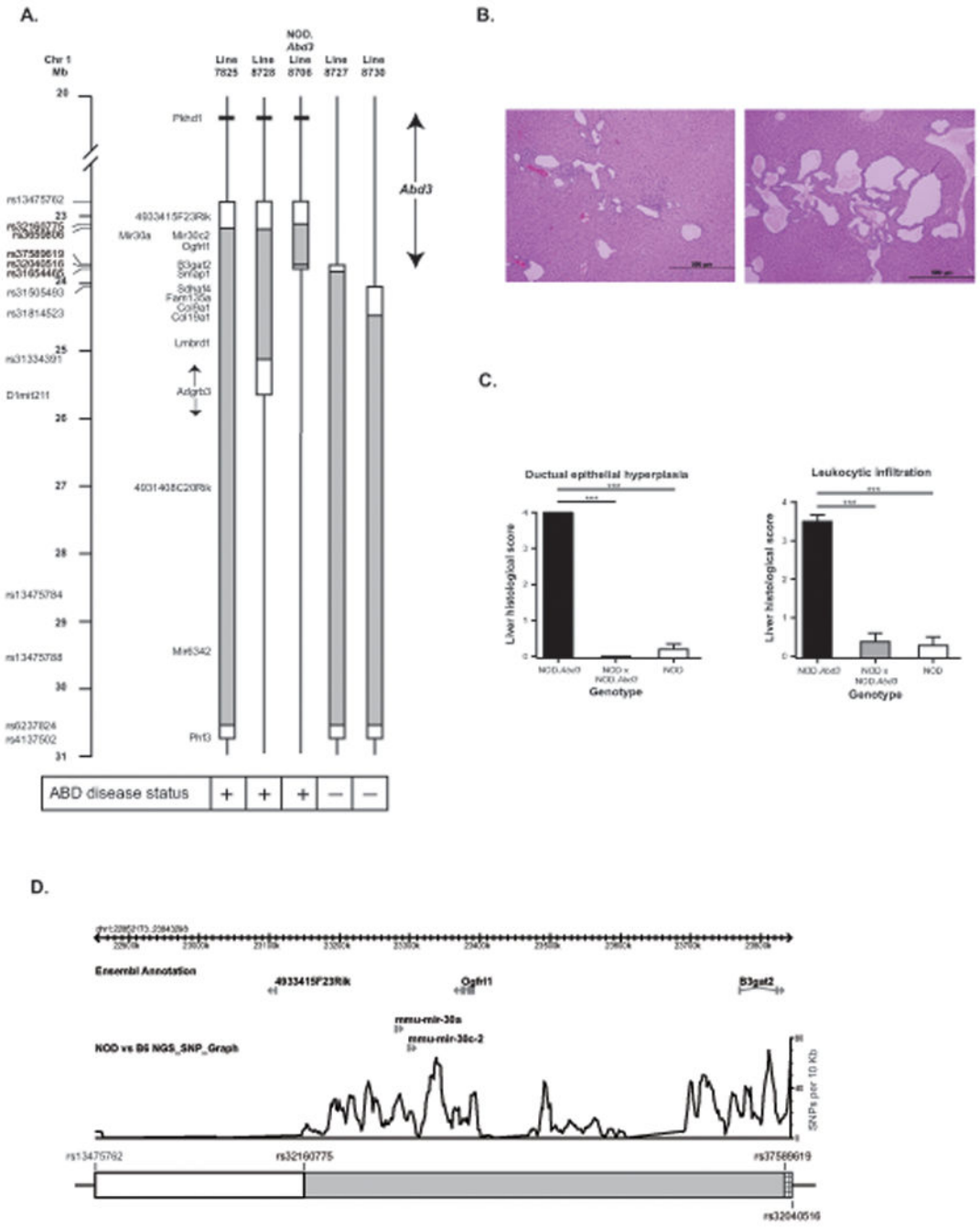

Figure 2. Congenic mapping defines the *Abd3* region as a recessive allele that controls clinical and microscopic ABD

A. Development of chromosome 1 "NOD.*Abd3*" congenic mice. Distal recombination events reduced the size of the *Abd3* region on chromosome 1 to a one Mb non-NOD congenic region and the mutated *Pkhd1* 2.5 Mb proximal to the congenic region (shown as a black bar). **B**. Histological disease (lymphocytic infiltration and biliary duct epithelial hyperplasia) develops in NOD.*Abd3* mice with the same kinetics/severity as in NOD.c3c4 mice (9). Representative H&E sections from NOD.*Abd3* mice aged 73 (left) and 120 days

(right). **C**. A single copy of *Abd3* is insufficient for disease in NOD.*Abd3* mice. No significant liver histology abnormalities in NOD.*Abd3* crossed to NOD (NOD: n= 10; NOD.*Abd3*: n = 10; NOD.*Abd3*×NOD: n = 22). All mice aged 120d. Mann-Whitney U test was performed for statistical significance. ***$P < 0.001$. Error bars displayed as SEM. **D.** Sequence comparison of NOD and B6 in the congenic portion of the *Abd3* region present in the NOD.*Abd3* strain. The schematic representation of the *Abd3* congenic region is shown at the bottom of the panel. The comparison of the B6 and NOD sequences (SNPs per 10 Kb) in the 1 Mb congenic portion of *Abd3* is shown in the middle of the panel. The genes within *Abd3* are shown at the top of the figure. Gray bars indicate B6.PL/B10-derived genome and white bars indicate where no NOD/B6 SNPs were genotyped. The thin solid lines indicate NOD genome.

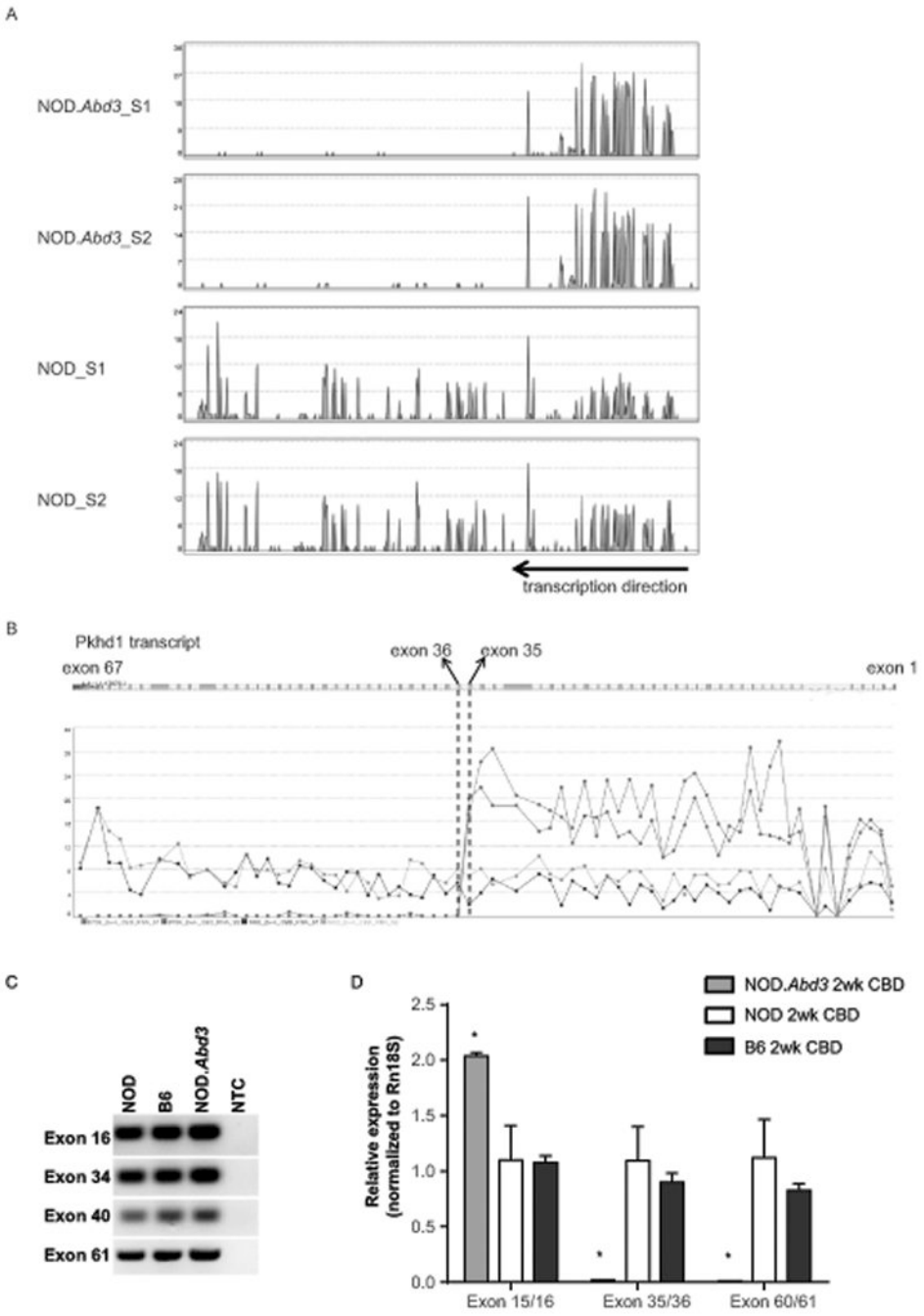

Figure 3. Abnormal *Pkhd1* expression pattern in NOD.*Abd3* CBD

A. Abnormal exon expression pattern of *Pkhd1*. RNA-seq reads aligned to reference C57BL/6 genome (mm9) show that expression of exons 36 to 67 of *Pkhd1* is absent in CBD of 2-week-old NOD.*Abd3* mice (upper two tracks) compared to NOD (lower two tracks). Each track represents one sample. Black arrow indicates transcription direction. **B**. NOD.*Abd3* CBD samples upregulate expression of exons 1-35. *Pkhd1* partition read density shown for two NOD.*Abd3* samples (red and blue dots) and two NOD samples (grey and brown dots). **C**. PCR using genomic DNA shows the presence of representative exons 16,

34, 40 and 61 in NOD, B6 and NOD.*Abd3* at DNA level. **D**. qRT-PCR confirms that NOD.*Abd3* CBD upregulates exon 15/16 expression and lacks exons 60/61 and 35/36 expression compared to NOD or B6. (N = 3/group, *: P<0.05 by student T test).

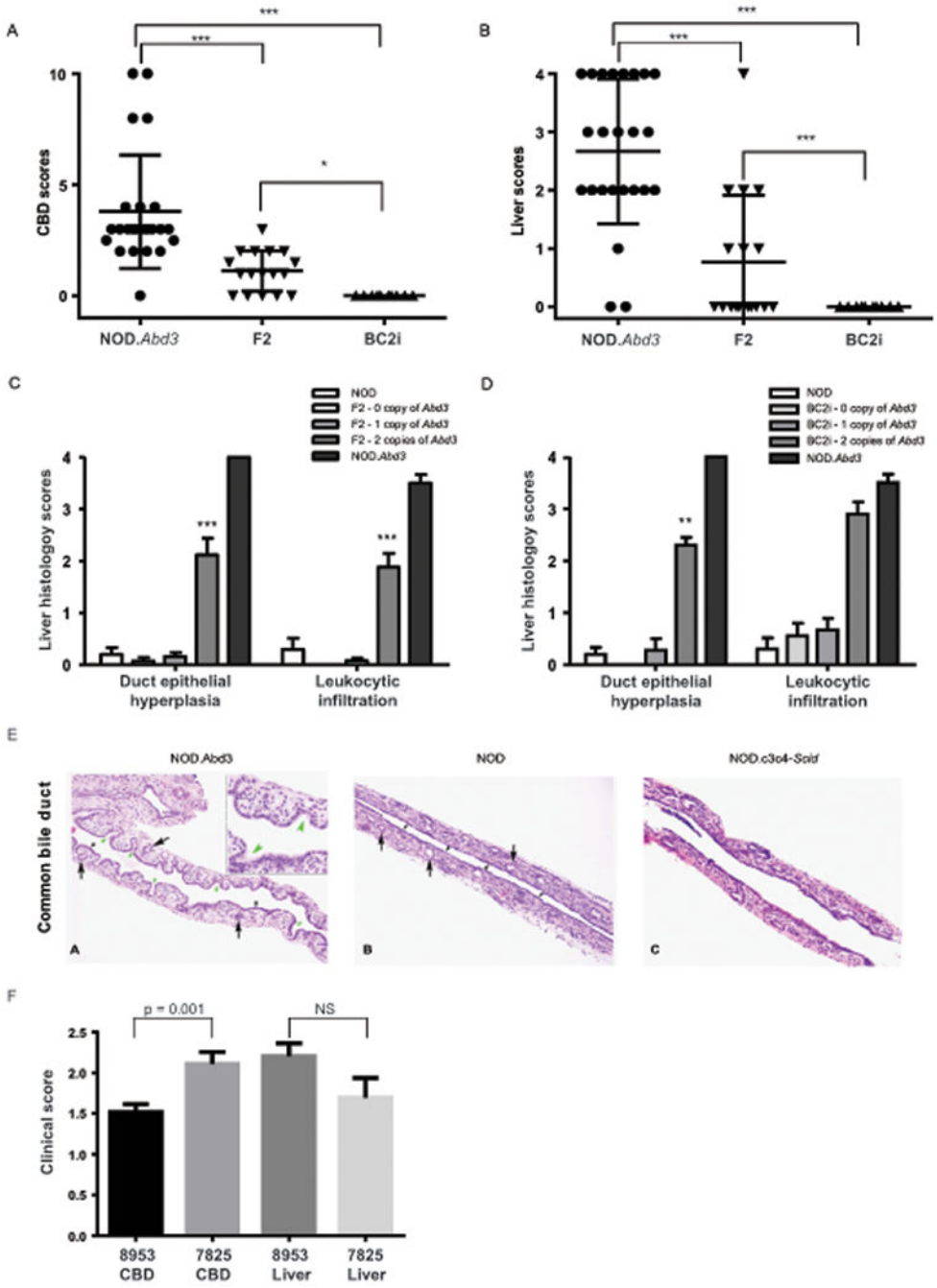

Figure 4. NOD genetic background is necessary for *Abd3* homozygosity to mediate autoimmune biliary disease; minimal role for the NOD MHC region

A, B. Clinical CBD and liver scores (see methods) of NOD.*Abd3* (n = 24), *Abd3* homozygous F2 (n = 17), and *Abd3* homozygous BC2i mice (n=10). Mann Whitney test performed for significance. ***$P < 0.001$; *$P < 0.05$. **C,D**. histology scores (see methods) of NOD (n = 10), NOD.*Abd3* (n=10), F2 and BC2i with 0, 1, or 2 copies of *Abd3* (F2 with 0 copy of *Abd3*: n = 14; F2 with 1 copy of *Abd3*: n = 25; F2 with 2 copies of *Abd3*: n = 17; BC2i with 0 copy of *Abd3*: n = 9; BC2i with 1 copy of *Abd3*: n = 18; BC2i with 2 copies of

Abd3: n = 10). All mice aged 120d. Mann-Whitney U test or Wilcoxon signed rank test was performed for statistical significance. $^{**}P < 0.01$; $^{***}P < 0.001$. Error bars displayed as SEM. **E**. 2-week-old NOD.*Abd3* mice showed substantial dilation of common bile duct (A) compared to age-matched NOD control mice (B) and NOD.c3c4-*scid* mice (C). Black arrow indicates peribiliary glands; green arrow indicates hyperplasia of biliary epithelium, consequently merging with peribiliary glands. Histology figures are representative of 6 CBD samples of NOD.*Abd3*, 6 CBD samples of NOD and 5 NOD.c3c4-*scid* mice at 2 weeks of age. **F.** Minimal role for the NOD MHC region in ABD pathology. Strain 7825 mice were bred to NOD.$H2^b$ mice in order to generate mice expressing *Abd3* on the NOD genetic background, but with a non-NOD MHC region (strain 8953, see methods). Strain 8953 mice (N= 30) and 7925 mice (n= 23) were aged to 120 days then assessed for clinical liver and CBD scores as above.

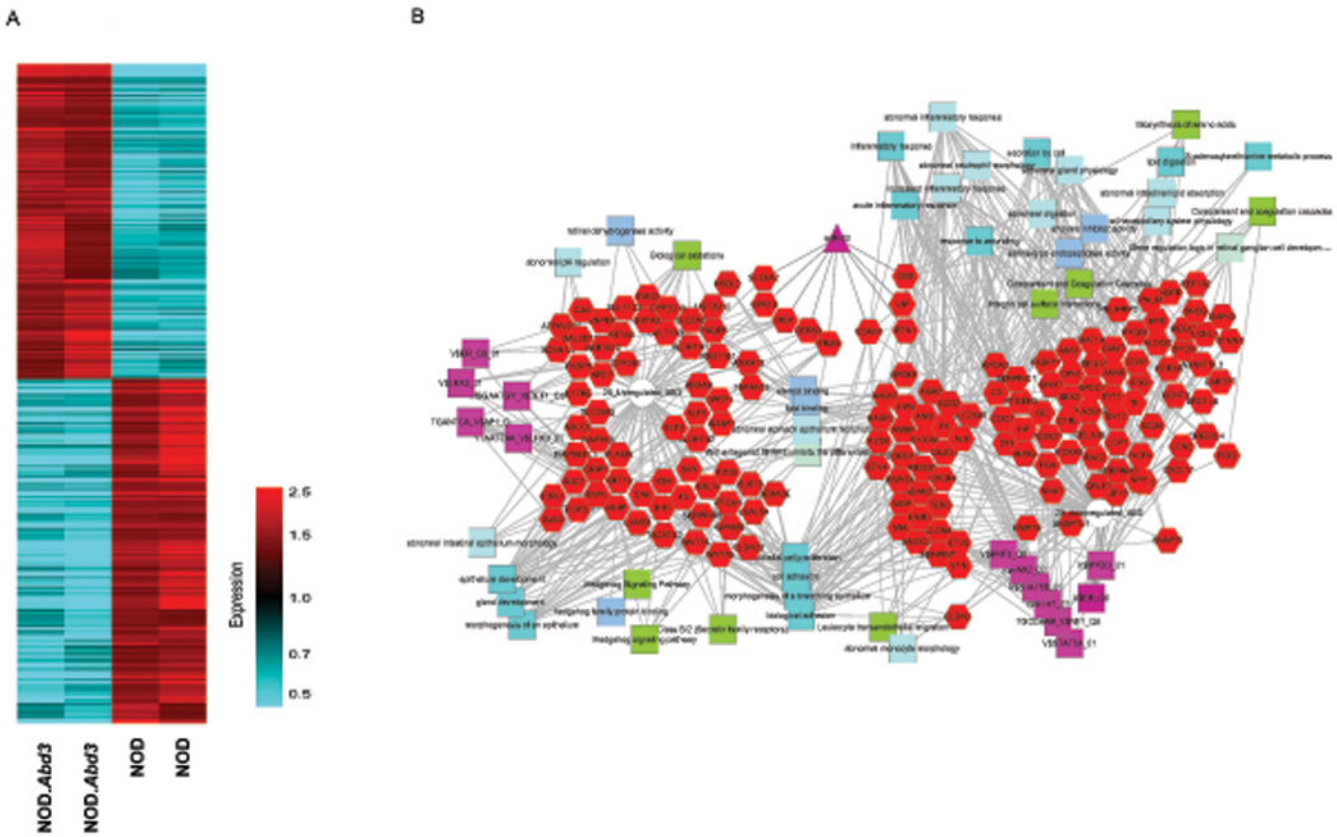

Figure 5. RNA-seq of 2-week-old NOD.*Abd3* common bile duct demonstrates upregulation of cholangiocyte damage response genes and downregulation of immune-related genes

A. Heatmap of 255 genes with at least two-fold change and significantly different expression (see methods) in NOD.*Abd3* compared to NOD CBD. **B**. Significantly differentially expressed genes from A were used to build a cluster enrichment network. Red hexagons represent genes; squares represents biological process (cyan), molecular function (sky blue), mouse phenotype (light blue), pathways (green) and transcription binding site (purple); triangle represents miR-30a. The left cluster represents the 2-fold upregulated genes and is highly enriched in cholangiocyte damage response genes; the right cluster represents 2-fold downregulated genes and is highly enriched in immune-related genes.

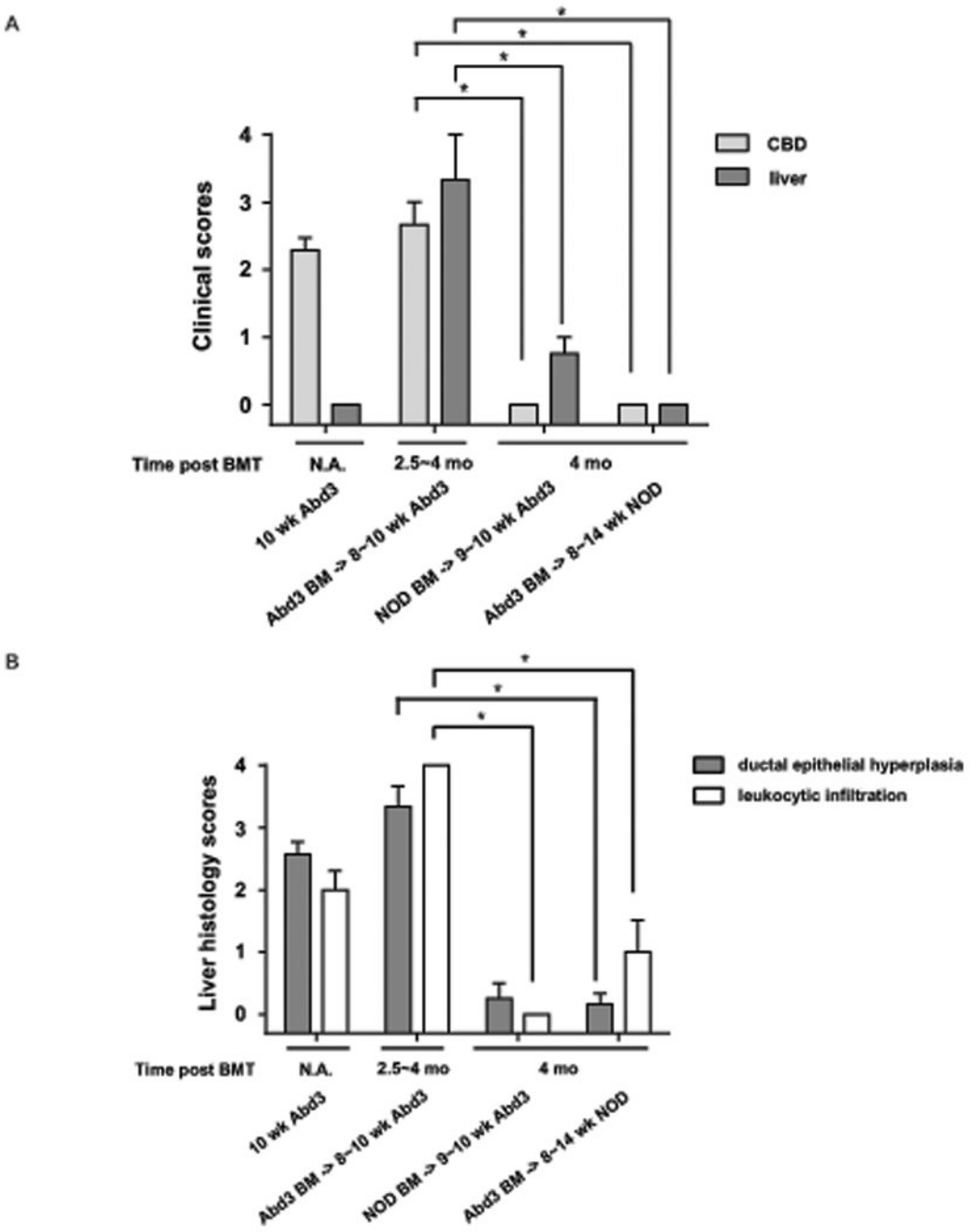

Figure 6. Bone marrow chimera studies show that *Abd3* expression is necessary in both the recipient (non-hematopoietic tissue) and in the donor (hematopoietic tissue) to recapitulate disease

Clinical CBD and liver scores (**A**) and histological scores (**B**) of: NOD.*Abd3* at 10 weeks (n = 7); NOD.*Abd3* recipients of either NOD.*Abd3* (n = 3, recipients were 8 to 10 weeks old at the time of BMT) or NOD bone marrow (n = 4, recipients were 9 to 10 weeks old at the time of BMT), and NOD recipients of NOD.*Abd3* bone marrow (n = 6, recipients were 8 to 14 weeks old at the time of BMT). *: $p<0.05$, by Mann-Whitney U test. Error bars represent SEM.

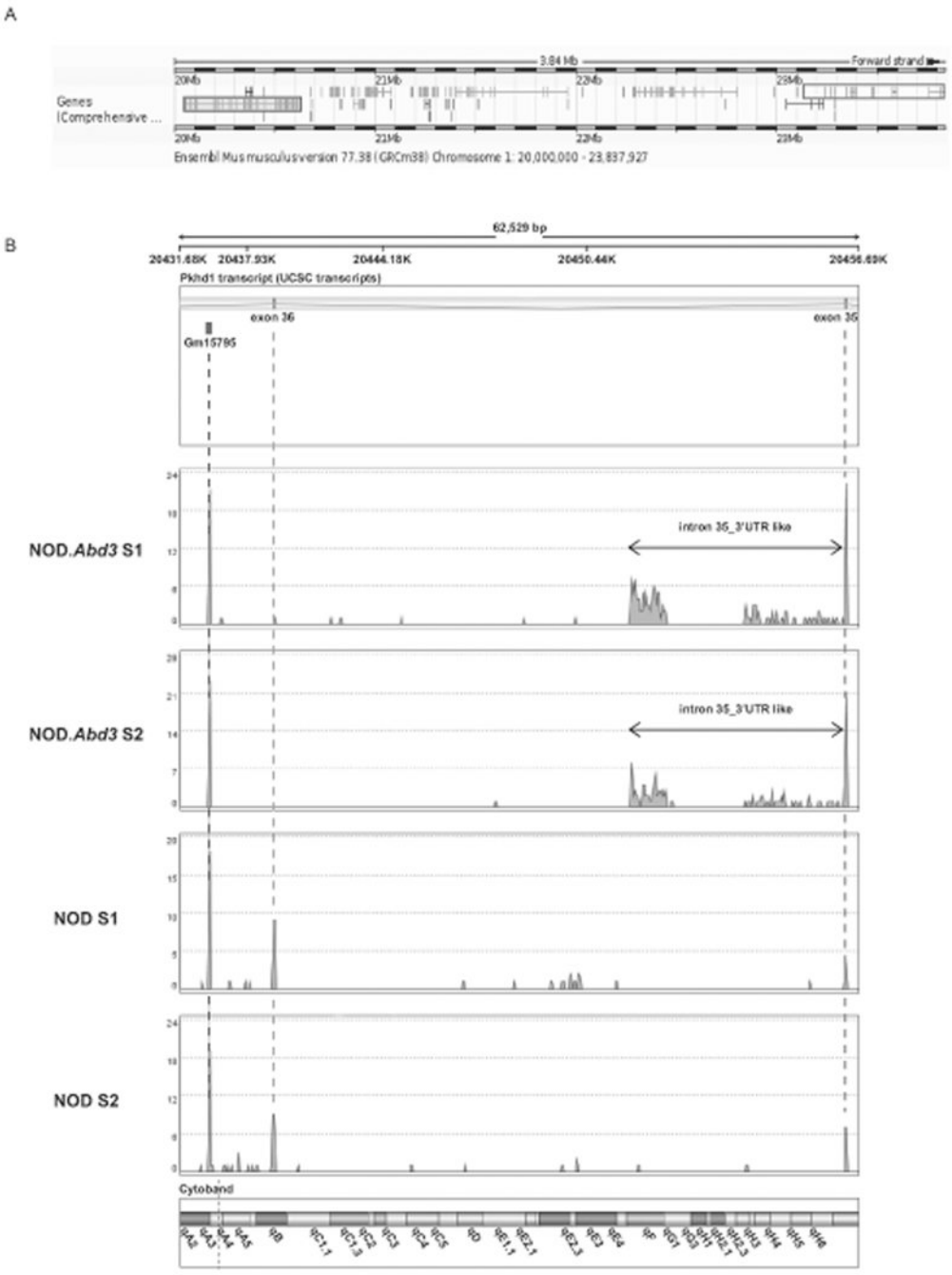

Figure 7. RNA-seq data reveals early termination of *Pkhd1* transcription in NOD.*Abd3* CBD

A. Genomic organization of *Pkhd1* and *Abd3* alleles. Blue and red boxes indicate *Pkhd1* gene and the B6/B10 *Abd3* congenic region, respectively. The *Pkhd1* gene and the *Abd3* region are ~2.5 Mb apart.

B. Magnified view of read-alignment from CBD RNA-seq data in the intron between exons 35 and 36 of *Pkhd1* comparing NOD and NOD.*Abd3* samples shows unique expression in NOD.*Abd3*. Red, green and blue dashed lines indicate the position of exon 35, 36 and the predicted pseudogene Gm15795, respectively, across all four RNA-seq tracks.

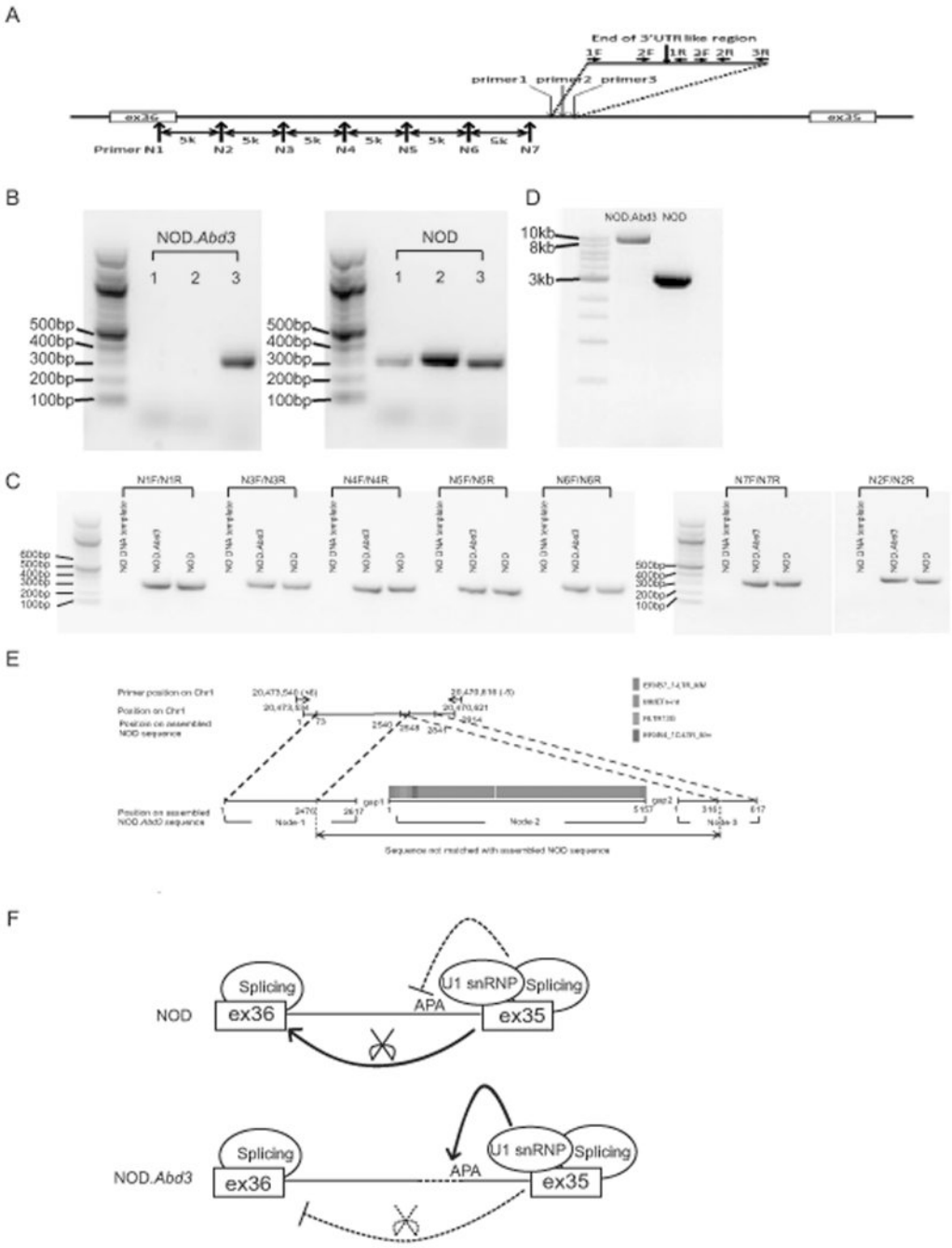

Figure 8. Mutation characterization of *Pkhd1* in NOD.*Abd3* and proposed mechanism of deficient NOD.*Abd3 Pkhd1* exon expression pattern

A. Schematic showing strategy of PCR primer design in intron 35 of *Pkhd1*. **B**. Primer 1 and 2 failed to amplify using NOD.*Abd3* genomic DNA while primer 3 successfully amplifies using both NOD.*Abd3* and NOD genomic DNA. **C**. Primers N1, N2, N3, N4, N5, N6 and N7 were all able to amplify the PCR product with expected product size using NOD.*Abd3* and NOD genomic DNA. **D**. Long-range PCR using primer N7 forward primer and primer 3 reverse primer showed distinct product sizes on NOD.*Abd3* and NOD genomic DNA. **E**.

Schematic representation of assembled long-range PCR product sequence in NOD and NOD.*Abd3* with relative position of the primer pair. Three nodes of *de novo* assembly were generated for NOD.*Abd3* with two small gaps present in between node-1/node-2 and node-2/node-3. Part of node-1 and node-3 can be matched with NOD assembled sequence and the rest of the NOD.*Abd3* assembly matches a class II ERV. Genomic positions of the primers and the sequences are based on C57BL/6 NCBI37/mm9 assembly. **F**. Schematic representation of potential mechanism of truncated *Pkhd1* transcript in NOD.*Abd3* CBD. APA: alternative polyadenylation site.

J Immunol. Author manuscript; available in PMC 2018 July 01.

Table One

Biological processes associated with significantly differentially expressed genes in NOD.*Abd3* CBD

Processes in which all genes are upregulated:			
ALDH1A1	PTCH1	ALDH1A1	CA9
ALDH1A2	SDC1	ALDH1A2	ELF3
CA9	SEMA3E	CA9	IL17RE
CERS3	SERPINB5	FRZB	KLF5
ELF3	SFN	FZD5	KRT19
EVPL	SLC26A3	HHIP	SLC26A3
F2RL1	TACSTD2	IHH	
FRZB	TFCP2L1	PTCH1	
FZD5	UPK1B	SEMA3E	
HHIP	WNT7A	SERPINB5	
IHH	WNT7B	TACSTD2	
KLF5	XDH	WNT7A	
PLAUR		WNT7B	

Processes in which all genes are downregulated:						
A4GNT	HPX	CLDN2	ALB	FGG	ALB	ALB
C3	HTR3A	CXCR4	ANG	PLA2G1B	AQP5	APOC1
CBS	MAT1A	NCF4	APOA2	SCG5	C3	C3
CORO1A	PTGER3	VCAM1	CARTPT	SNAP25	CARTPT	CBS
CPN1	S100A9		F5	SNCG	CDO1	HPX
CUZD1	SERPINC1		FGA	SYCN	CUZD1	MAT1A
CXCR4	SPDEF		FGB	SYT7	GC	NGFR
EEF1A2	SYCN				HPN	REG1B
FKBP11	SYT7				HTR3A	SERPINC1
GCNT3	VIP				SNAP25	

Processes in which all genes are downregulated:						
					SYCN	
					VIP	

Processes in which genes are up- and downregulated:				
biological adhesion		**cell adhesion**		**epithelial cell proliferation**

[1]Biological process enrichment analysis shows the significantly differentially expressed genes in CBD from 2 week old mice (from Figure 5A) associated with biological processes characterized by upregulated genes (red font) and downregulated genes (green font). The biological processes characterized by all upregulated or downregulated genes are in green and red respectively. The processes involving some up and some down regulated genes are in black font and the individual genes are in green or red type depending on whether they are up or downregulated.

Table Two
PCR amplification result of different primer pairs

Primer set or exon position	Starting position*	Ending position*	Amplification of NOD.*Abd3*	Amplification of NOD
Exon 36	20,440,302	20,440,458	NA	NA
Primer N1	20,440,373	20,440,692	Yes	Yes
Primer N2	20,445,607	20,445,925	Yes	Yes
Primer N3	20,450,397	20,450,733	Yes	Yes
Primer N4	20,455,542	20,455,846	Yes	Yes
Primer N5	20,460,303	20,460,626	Yes	Yes
Primer N6	20,465,591	20,465,989	Yes	Yes
Primer N7	20,470,616	20,470,976	Yes	Yes
Primer 1	20,472,908	20,473,208	No	Yes
Primer 2	20,473,134	20,473,447	No	Yes
Primer 3	20,473,238	20,473,540	Yes	Yes
Exon 35	20,493,023	20,493,173	NA	NA

*Genomic coordinates refer to Chromosome 1. genomic assembly: NCBI37/mm9. Yes: single band with expected PCR product size; No: no band shown on the gel; NA: no PCR was performed.